NAA-SR-7875
INSTRUMENTS
49 PAGES

DYNAMIC VOID FRACTION MEASUREMENT SYSTEM

By

J. H. KENDRON
E. E. STONER
G. M. TAYLOR

ATOMICS INTERNATIONAL

A DIVISION OF NORTH AMERICAN AVIATION, INC.
P.O. BOX 309 CANOGA PARK, CALIFORNIA

CONTRACT: AT(11-1)-GEN-8
ISSUED: MAY 15, 1963

DISCLAIMER

DISTRIBUTION

This report has been distributed according to the category "Instruments" as given in "Standard Distribution Lists for Unclassified Scientific and Technical Reports" TID-4500 (19th Ed.), August 31, 1962. A total of 680 copies was printed.

CONTENTS

TABLE

FIGURES

ABSTRACT

Various methods and techniques of measuring void fraction in boiling heat transfer media are discussed. Details of 17 void fraction measurement systems are abstracted.

A dynamic void fraction measurement system is described, capable of continuously measuring void fraction at any position along a 12-ft test section.

Void fraction (the ratio of vapor volume to total volume of a 2-phase mixture) is measured in boiling organic coolant contained by a test section of 5/8-in. -OD nickel tube with 0.049-in. wall thickness. Measurement of void fraction without physical contact with the test section is achieved through the use of a radiation attenuation method. The intensity of a narrow 100-kev x-ray beam transmitted through the test section is measured and recorded to permit calculation of void fraction. An x-ray tube and scintillation detectors are mounted on a remotely controlled elevator assembly used for horizontal and vertical positioning. Major sources of measurement error due to fluctuations in x-ray tube output and fluctuation of detector power supply voltage are cancelled by using two detectors connected in a differential circuit. Detector cooling and heavy magnetic shielding further reduce measurement errors. Typical measurement accuracies for small and large void fractions are 0.05 ± 0.015 and 1.00 ± 0.022.

I. INTRODUCTION

An area of major concern in power reactor operation is the danger of inhibiting the flow of the reactor coolant channels below acceptable levels. Inadequate cooling of the reactor core can lead to fuel element destruction and the subsequent potential hazards associated with release of fission products. Inadequate cooling may occur in reactors during a loss-of-pressure accident, resulting in bulk boiling. When such boiling occurs in a reactor channel, increased resistance to flow in that channel causes a decrease in the flow rate, resulting in increased boiling. This, in turn, causes further decrease in flow rate and may lead to flow-choking.

The aim of the Pressure Transients and Flow Stability Project,[39] part of the Atomics International Reactor Safety Program, is to investigate, both analytically and experimentally, the effects of loss-of-pressure accident in organic cooled reactors. This study is required to improve the accuracy and the reliability of present organic coolant analytical models used in the hazards evaluation of the accident.[40] Closely interrelated with an adequate evaluation of the loss-of-pressure accident is the ability to predict the void fraction (ratio of vapor volume to total volume of a 2-phase mixture) of the coolant during subcooled and bulk boiling. Consequently, the experimental investigation of organic coolants void fraction has been included in the experimental effort of the Pressure Transients and Flow Stability Project.

Specifically, this report describes the development of equipment to continuously measure void fraction over a representative range of steady state boiling conditions for typical organic coolant, flowing in a heated channel at low system pressures. In addition, void fraction measurements are also required for transient boiling conditions as induced in the heated channel by a gradual depressurization of the system (simulated loss of pressure accident).

The above requirements plus ability to scan the heated channel along its length and width constitute the basic operational specifications for design of the void fraction measuring system described in this report. Measurement accuracy of ± 0.05 void fraction was established as a minimum acceptable limit for the experimental investigation.

A. METHODS OF MEASURING VOID FRACTION

Void fraction determination of a 2-phase mixture may be obtained through either of two measurement philosophies:

1) Direct Measurement – actual volumetric measurement of the gas phase, and

2) Indirect Measurement – measurement of some property of the 2-phase mixture from which the void fraction can be inferred.

For each of these basic measurement philosophies, a number of techniques have been suggested or tried.

1. Direct Measurement Techniques

a. Visual Observation

High speed photographs are taken through a transparent test section containing a 2-phase mixture. The number and size of the bubbles appearing on the photograph give a direct indication of the void volume and hence the void fraction within the test section.

b. Volumetric Flow

Volumetric flowmeters are located at the inlet and outlet of the test section. The inlet flowmeter indicates the liquid volumetric flow rate, while the outlet meter indicates the liquid-plus-gas volumetric flow rate. The instantaneous difference in flowmeter readings is a direct indication of the volumetric gas flow rate. If this quantity is divided by the inlet flow rate, the result is the average value of void fraction for the entire test section.

c. Quick-Closing Valves

Simultaneously operated quick-closing valves located at the inlet and outlet of the test section are used to entrap the boiling liquid. After sufficient separation time, the liquid level in the test section is measured. Knowing the total length of the test section, the average void fraction may be easily calculated.

2. Indirect Measurement Techniques

Since density of a 2-phase (liquid-vapor) mixture is almost inversely proportional to void fraction, and is relatively easily measured, most investigators have used density measurement techniques. Many methods exist for

determining density by measurement of various properties of the mixture such as absorptivity of vibrational energy, dielectric constant, resistivity, permeability, attenuation of radiant energy, and absorption of radioactive particles. Various density measurement techniques are discussed in the appendix literature survey.

B. DISCUSSION OF MEASUREMENT TECHNIQUES

Selection of a void fraction measurement method requires consideration of the following factors: (1) test section characteristics, (2) coolant characteristics, (3) operating temperatures and pressures, (4) measurement accuracy, resolution, and stability, and (5) response time of measurement system.

The test section used for the flow stability test loop consists of a 12-ft length of 5/8-in.-OD nickel tube with a wall thickness of 0.049 in. The coolant, Santowax R, is an opaque, yellowish wax-like substance at room temperature and becomes liquid with a density of about 63 lb/ft^3 at 300°F. The test loop is operated at temperatures up to 750°F and pressures up to 50 psig. Void fraction measurement accuracy of about ±5% was based on the accuracy of other measurements (temperature, flow, and pressure) with which the void fraction measurements are correlated.

To study flow and pressure transients, the response of the void fraction measurement system should be about 1 to 10 msec. The measurement system should be capable of measuring localized void fraction at any position along the length of the test section. It is desirable that the measurement system be capable of longitudinal and transverse automatic scanning of the test section for the purpose of void fraction distribution studies. A rectangular beam of 0.5 by 0.1 in. was chosen to permit transverse scanning of the test section. Direct measurement techniques either could not be used or would not satisfy the established requirements for the void fraction measurement system.

An investigation of density measuring techniques indicated that many of these techniques are strongly dependent on the distribution of the vapor phase in the liquid phase, or necessitate the use of some form of signal which affects the phenomena under investigation.

Ultrasonic density measurement techniques were considered, but the possibility of affecting bubble growth with vibrational energy and the apparent difficulty of adapting this technique to a 5/8-in. -diameter test section at 750°F suggested that a better method be found. The physical properties of the test section and coolant discouraged the use of dielectric constant, resistivity, and permeability measurement methods. These measurements would require the use of small, electrically insulated probes penetrating through the test section into the coolant. Dielectric constant probes of the size which could be installed in the test section would require a measurement resolution of ±0.032 $\mu\mu$f to measure void fraction with an accuracy of ±0.05%. Although this type of measurement could be conducted under laboratory conditions, it would be very difficult and costly to do in the test section environment. Resistivity measurements of the organic coolant, with a resistivity of 10^9 ohm-cm, would be impossible to accomplish with the accuracy required because of the strong dependence on vapor-liquid phase distribution. Permeability measurements of the organic coolant, with a very low relative permeability, in the presence of the nickel test section with a very high permeability, would yield no useful information.

Particle absorption measurements could not be used because of the wall thickness and density of the test section. Calculations of beta source energy requirements showed that a source located externally to the test section must emit particles with energies greater than 10 Mev to penetrate the test section. An internal beta-emitting isotope mixed with the coolant must emit particles with an energy of over 4 Mev in order to penetrate the test section. Isotopes having these beta energies are not available.

Radiation attenuation methods were investigated and appeared to be the only way with which to measure void fraction under the existing test loop conditions and to meet the requirements established for the void fraction detection system. Initial radiation attenuation calculations indicated that any x- or gamma-ray with an energy over 50 kev would penetrate the test section without an unreasonably high degree of attenuation (< 100/1).

An optimum radiation energy of 80 to 110 kev was established as the result of a series of compromises among several competing factors, i.e., measurement resolution, source availability, and vapor-liquid phase distribution error.

II. DESCRIPTION

A. GENERAL FEATURES

The void fraction detector consists of an x-ray tube photon source, collimators, water-cooled scintillation detectors, and position transducers; all mounted on an elevator assembly which permits scanning the test section either vertically or horixontally. Located outside of the test section enclosure are: the x-ray control console and high voltage power supply, the elevator control panel, the detector control panel, detector power supply, differential amplifier, X-Y recorder, and line voltage regulators. This test loop instrumentation is shown in Figure 1.

The x-ray beam is split into two narrowly collimated beams. The top view of the collimator arrangement is shown in Figure 2. A side view of the detector collimator arrangement is shown in Figure 3. One beam is transmitted through a dummy or reference test section filled with Santowax R, at room temperature. A cross section of the test section and support structure is shown in Figure 4. The other beam is transmitted through an electrically heated test section. A dc signal voltage from each of two scintillation detectors, located behind each test section, is fed into a differential amplifier whch subtracts the reference signal from the void fraction signal. The purpose of the reference signal is to reduce the effects of fluctuating high voltage to the detectors and fluctuation in x-ray tube output. The dc output signal from the differential amplifier drives one axis of an X-Y recorder, and a high speed recording oscillograph, which are calibrated to read void fraction. The void fraction detector block diagram is shown in Figure 5.

B. PHOTON SOURCE

A lower energy limit for the photon source was established on the basis of the radiation attenuation characteristics of the nickel walled test section. As photon energy decreases below about 200 kev the total mass absorption coefficient, and hence the radiation attenuation by the nickel test section, begins to increase rapidly. Below 100 kev there is a nearly exponential increase in attenuation as energy is decreased. At 50 kev a beam of photons is attenuated by a factor of about 100/1 by the walls of the test section. For these reasons, a source energy of 50 kev was established as a practical lower limit.

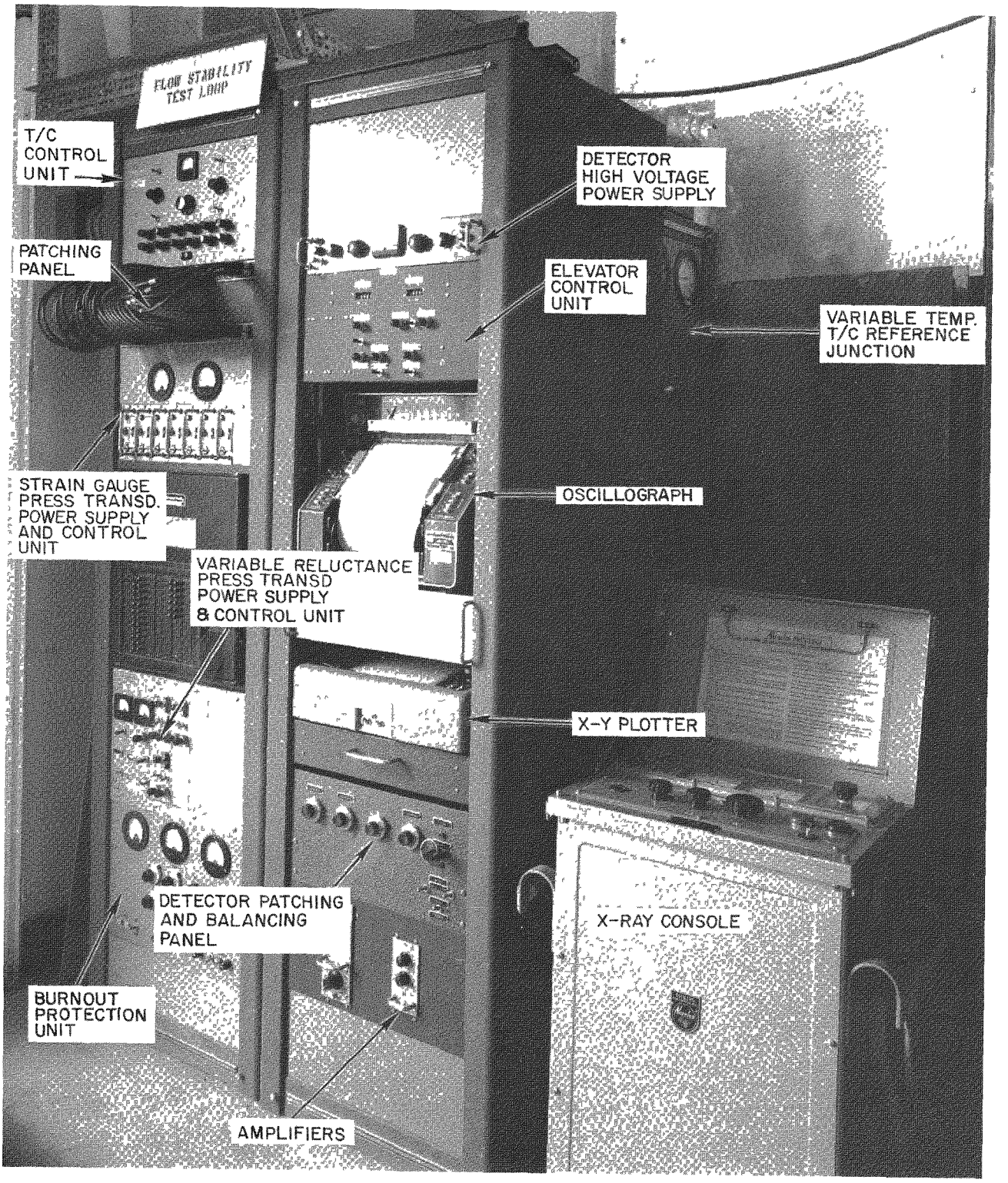

7549-5438A

Figure 1. Test Loop Instrumentation

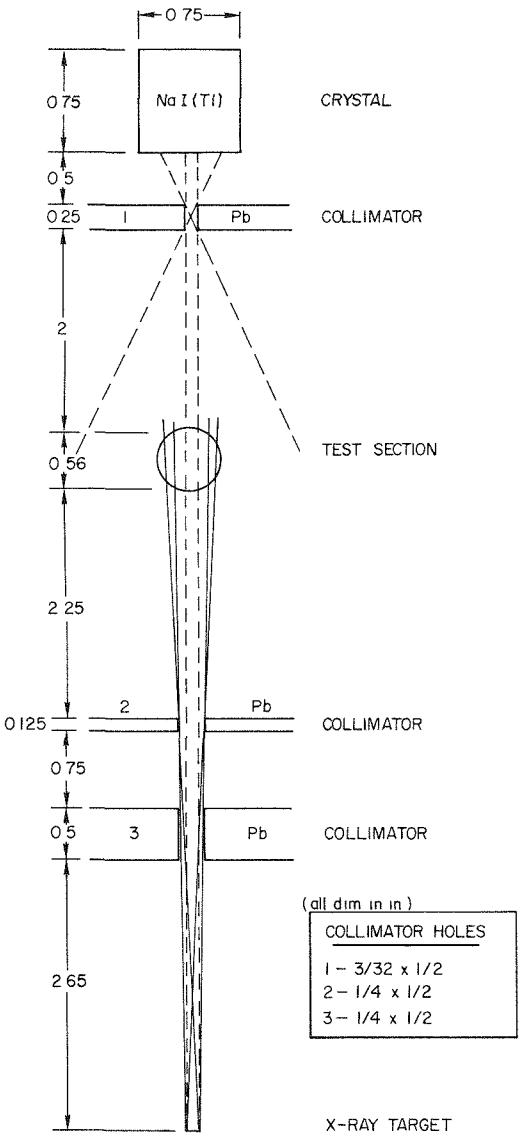

Figure 2. Collimator Arrangement (Top View)

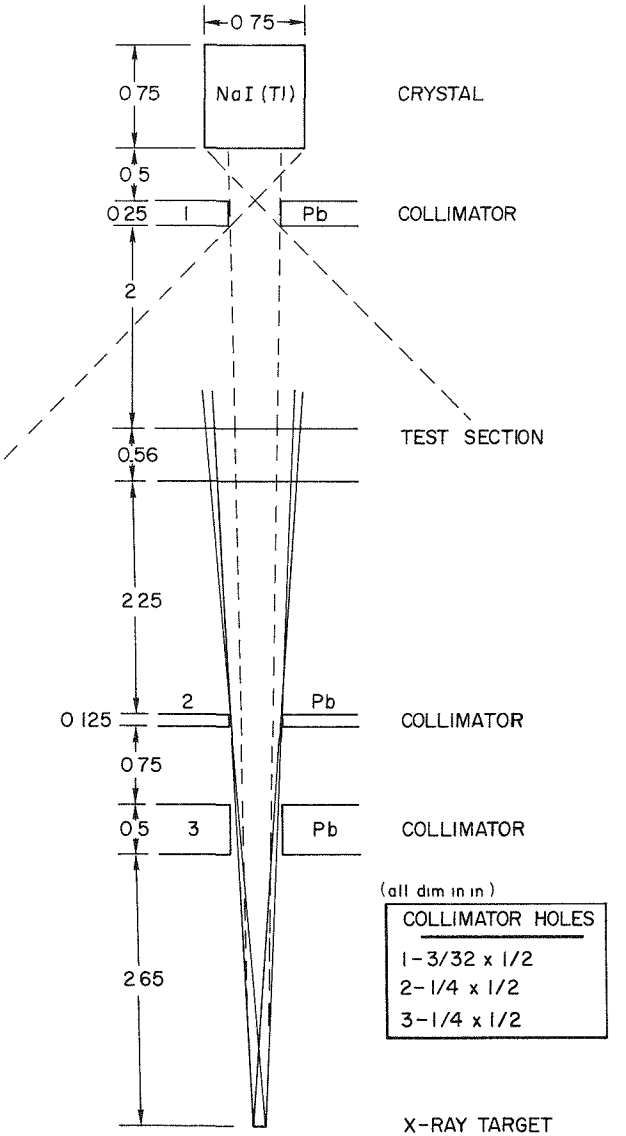

Figure 3. Detector Collimator Arrangement (Side View)

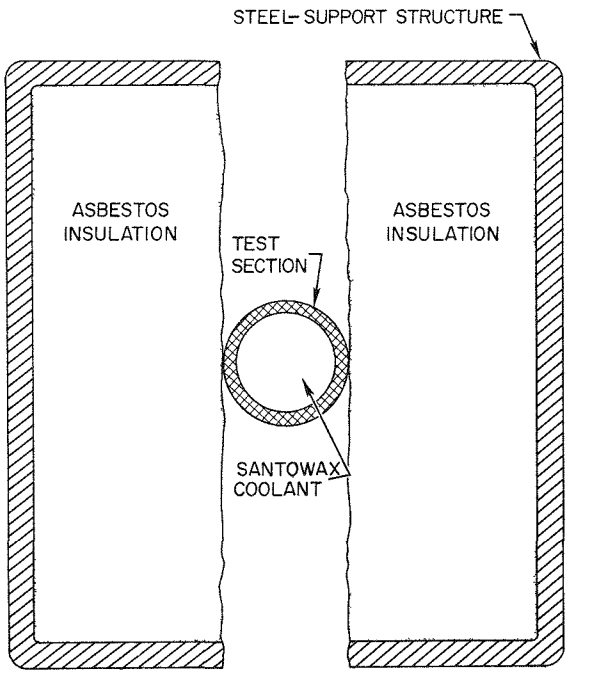

TEST SECTION SEAMLESS NICKEL TUBING, 0.479-in ID WITH 0 049-in. WALL THICKNESS

Figure 4. Cross Section of Test Section and Support Structure

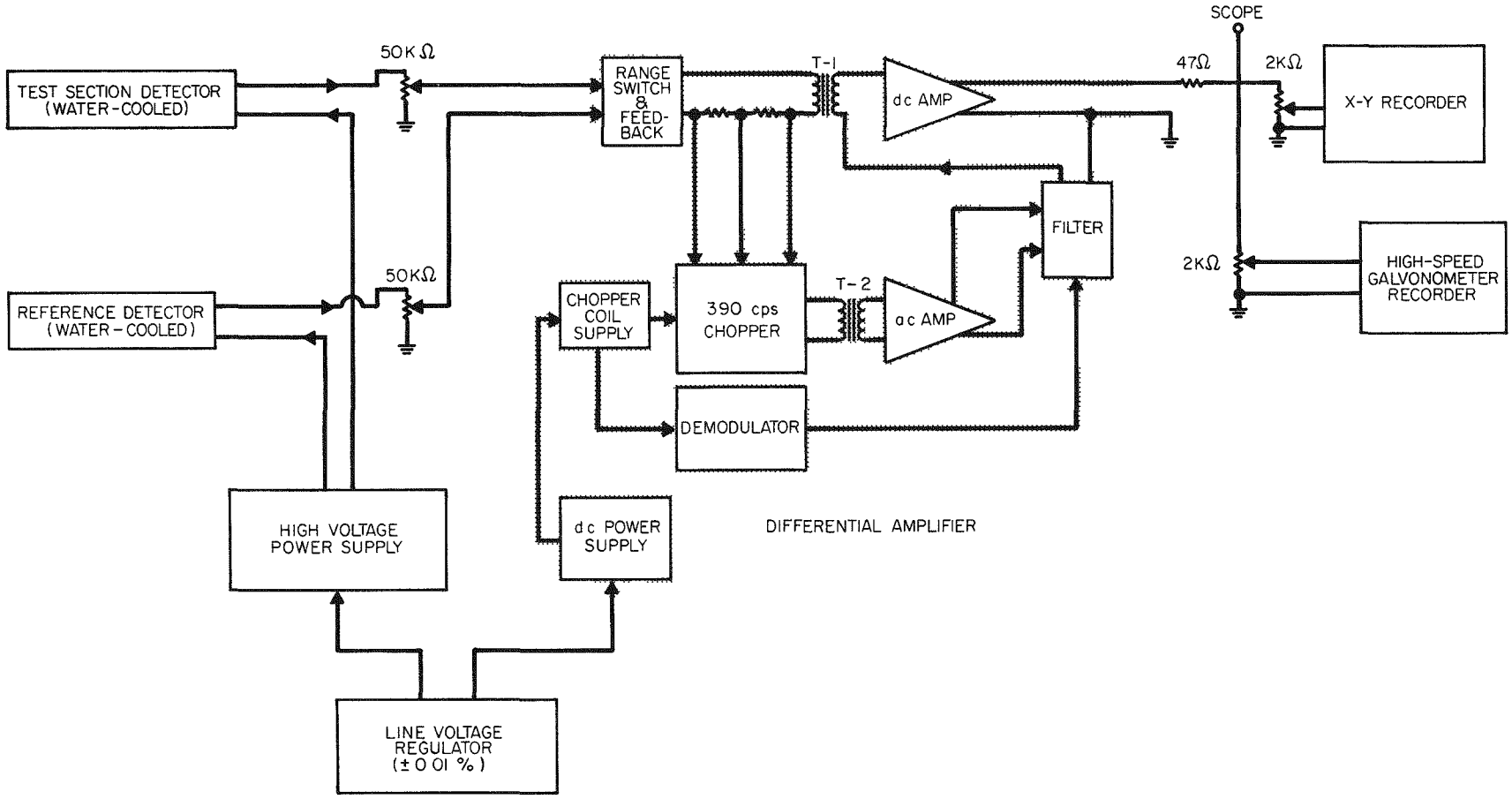

Figure 5. Void Fraction Detector Block Diagram

The high energy limit for a photon source was determined by considering the radiation attenuation characteristics of the coolant, and the ability of the measurement system to accurately measure a signal change corresponding to a change of void fraction of ±5%. (As the energy of the radiation source increases, the change in attenuation of the coolant, due to a given void fraction change, decreases). A reasonable estimate of the measurement error of a well designed radiation intensity monitoring system appears to be about 1 to 3%. The energy at which a ±5% change of void fraction results in a signal or attenuation change of less than 3% occurs at photon energy under 150 kev. The maximum energy of the photon source was therefore set at about 150 kev.

Optimum photon source energy was determined by considering the measurement error caused by various bubble orientations. When the mean attenuation length of the coolant is less than the coolant channel thickness, the radiation intensity of the beam entering the detector will depend not only on void fraction but also upon bubble orientation. The most serious bubble orientation errors arise when comparing bubble sheets with bubble slugs at 50% void fraction.[19] If the photon source energy is set so that the attenuation coefficient of the coolant is considerably less than 1, the measurement error due to bubble orientation becomes very small. The optimum source energy was established at about 100 ± 20 kev, where the measurement error due to the most extreme bubble orientation problems is equal to the error of the measurement system (about 1 to 20%).

To achieve the statistical accuracy necessary for measuring void fraction of 5% in 1 to 10 msec, the radiation intensity at the detector must be about 10 to 100 r/hr. Thus a 50-kev source would require an intensity of from 1000 to 10,000 r/hr.

In the energy range of interest, there is only one isotope available which can be obtained with a high specific activity and a half-life which is long enough to permit its use. This isotope is thulium-170 (half-life = 129 days) which can presently be obtained with specific activities of about 100 c/gm. The Tm^{170} spectrum consists of a continuous background of Bremsstrahlung due to the slowing down and stopping of electrons emitted by Tm^{170}. Superimposed on the background are two peaks due to decay of the ytterbium-170 (Yb^{170}), daughter of Tm^{170}. These peaks result from decay gamma-ray (84 kev, 3% yield) and K, x-ray (53 kev, 5% yield) transitions in the Yb^{170}. Although it is possible to obtain Tm^{170} sources of sufficient intensity to adequately perform the desired measurements, the cost of a 1-yr supply of sources is greater than the cost of an x-ray machine of comparable or greater output.

From technical data on small commercial x-ray generators in the 50- to 75-kev class, a beam of the desired shape and intensity could probably be generated at maximum operating conditions. However, because of the unknown accuracy of the manufacturer's claims of machine output, spectral distribution, and beam energy distribution, and the inherent difficulty in making precise measurements of these parameters, it was concluded that a 50-kev x-ray generator of the types investigated would only marginally meet our requirements. Of the x-ray generators in the 100- to 150-kev energy range, only constant potential machines were given serious consideration. The main reason for choosing a constant potential x-ray generator is, to eliminate the cyclic fluctuation in beam intensity and cyclic spectral shift which is an inherent characteristic of "rectified-unfiltered" generators. (Although the detection system was designed to eliminate the measurement error, due to small changes in x-ray beam intensity, caused by power line surges; it cannot compensate for the large intensity fluctuation of rectified-unfiltered x-ray machines).

Only two constant potential x-ray machines (Norelco and Muller) were found which satisfied both technical requirements and budgetary limitations. The Muller machine was procured on the basis of a cost advantage.

This device is the MG-150 industrial unit which is continuously adjustable in the ranges from 25 to 75 and from 50 to 150 kv-dc. Continuous rated output of the apparatus is 3 kw. An automatic line voltage correction unit maintains the incoming line voltage constant to within ±1.5% for voltage fluctuations up to ±40 v. The x-ray tube is a Norelco MG-150/1 double focus, beryllium window, 150 kv-dc tube. At a target-to-specimen distance of 3 in., the dose rate output is 6.9×10^6 r/hr, when operated at 100 kev and 18 ma. Focal spot sizes are 0.7 and 2.5 mm. During calibration of the void fraction detector, severe line voltage fluctuations caused a variation in x-ray machine output, which corresponded to a void fraction change of about 100%. This problem was solved by installing a Sola constant voltage transformer and a Stableline constant voltage regulator in tandem in the power line supplying the x-ray generator.

C. ELEVATOR ASSEMBLY

The elevator table consists of two plates separated from each other by ball-bearings and tracks. Rigidly attached to the bottom plate is a horizontal drive motor, reduction gears, left and right limit switches, and horizontal

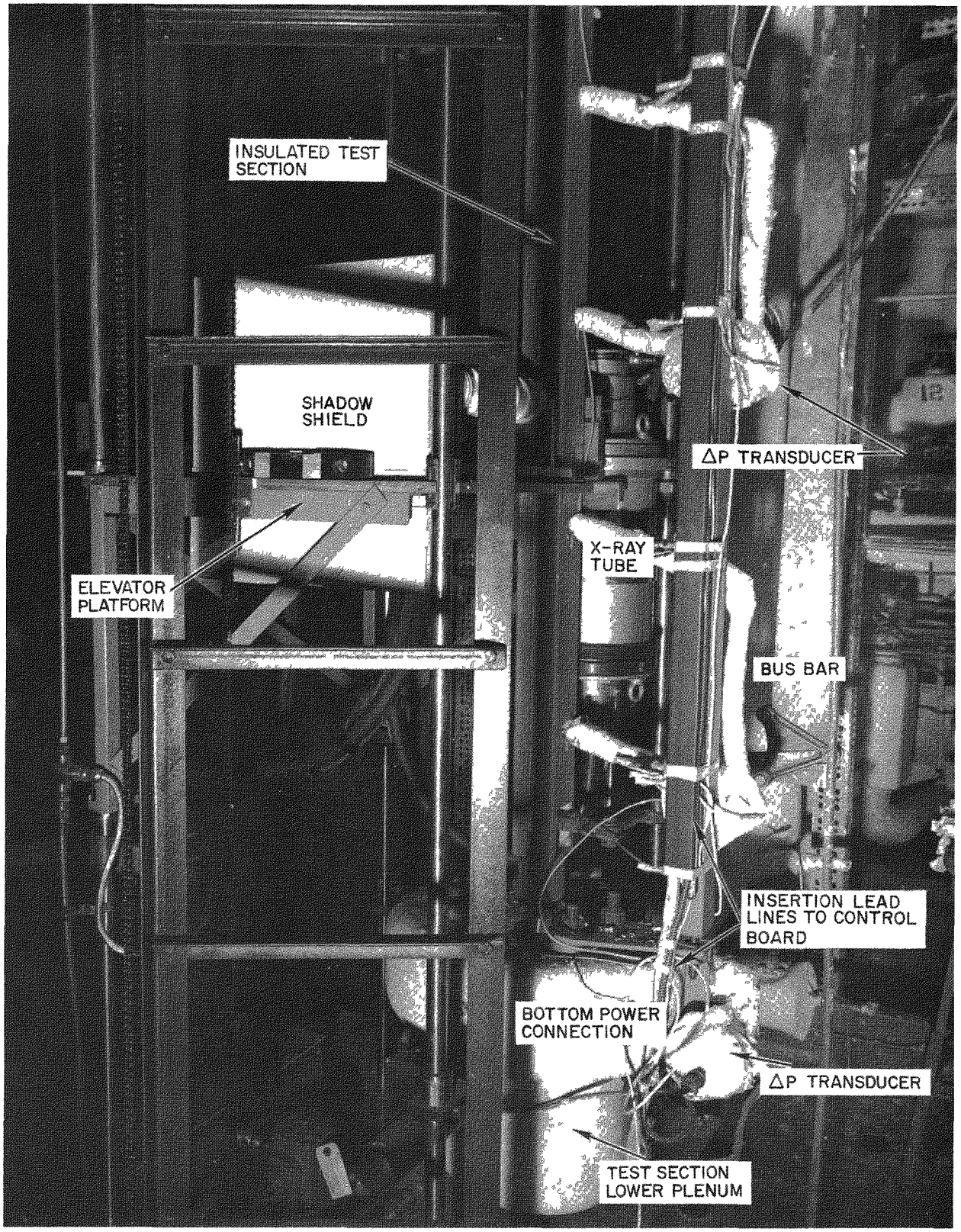

7549-5438B

Figure 6. Test Section Installation

position transducers. The x-ray tube, collimators, dummy test section, and shielding are mounted on the top plate. The horizontal drive motor is a bidirectional, capacitance motor, which is actuated by a remote (left-off-right) switch located on the elevator control panel. A screw and nut drive-device couples the motor and reduction gears to the top plate, transforming rotational to rectilinear motion. The test section installation is shown in Figure 6. The top plate has a total horizontal movement of 1 in. but can be adjusted to about 2 in. for horizontal scanning of rectangular test sections. Initially the elevator table is manually adjusted so that the narrow x-ray beam will pass through the center of the test section. The test section can then be remotely scanned horizontally ±0.5 in. on either side of the center line. Left and right limit switches stop the drive motor when the top plate reaches ±0.5 in. A synchro-position transmitter sends an electrical signal to a remote synchro-receiver unit located on the elevator control panel. Horizontal position is indicated in thousandths of an inch on a servo driven Veeder-Root counter. A 10-turn helipot, mechanically coupled to the gear train, provides an electrical position signal for the input to the X-Y recorder whenever plots of void fraction vs position are required. A complete horizontal scan of the test section takes approximately 15 sec.

The elevator vertical drive mechanism is essentially identical to the horizontal drive with the exception of a more powerful motor. A sprocket wheel and chain raises and lowers the elevator table. Counter weights were used to reduce drive power to that required to overcome friction only. The elevator can be stopped at any elevation simply by cutting off power to the drive motor. Vertical position transducers, which are identical to the horizontal transducers, are used to indicate vertical position to within 0.1 in. The elevator can be repositioned at a rate of 0.4 ft/sec.

The elevator table is guided by 4 vertical steel rods of 1-in. diameter. They are maintained rigid by means of struts which connect to the main test loop support structure and to the building beams. The elevator table rides the steel guide rods on partial ball bushings which clear the guide rod support struts. Because of the location of the x-ray tube at the edge of the elevator table, the center of gravity (CG) is displaced from the center of the table, resulting in an undesirable moment which would cause the elevator to bind. The CG is returned to the geometrical center of the table by means of lead counterweights.

The entire weight of the elevator table and counterweights is supported from above by means of steel reinforced pillow blocks which are fastened to an overhead building beam. The total weight of the elevator assembly is about 300 lb.

D. COLLIMATORS AND SHIELDING

The collimation system is illustrated in Figure 7. The small focal spot of the x-ray tube is used and the beam entering the detector is ~0.1 by 0.5 in. in cross section.

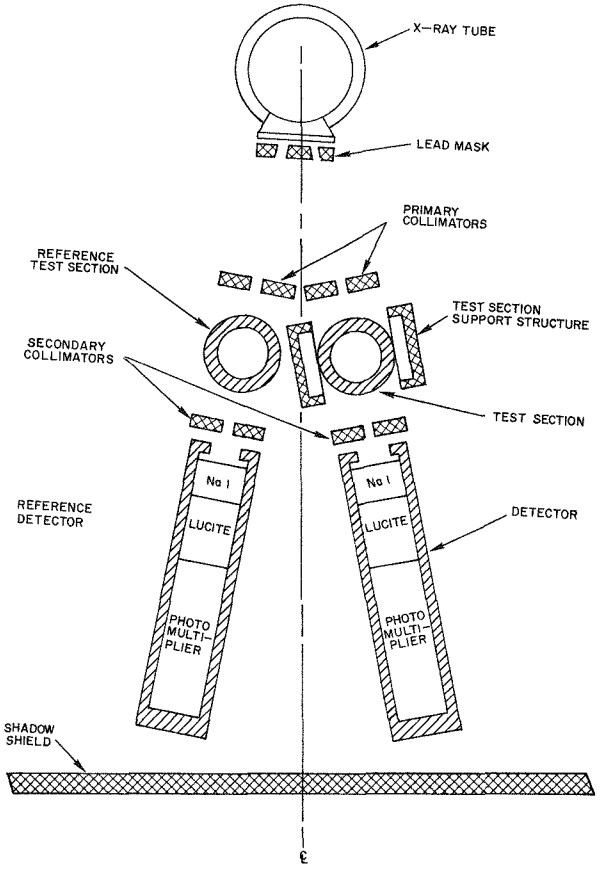

Figure 7. Collimator and Shielding

A 1/4-in.-thick lead shadow shield is placed behind the detectors to minimize the radiation escaping the test section enclosure. The maximum measured dose rate at the surface of the test loop enclosure is about 3 mr/hr. At any of the operating positions or locations where personnel normally work, the radiation is not detectable.

E. INSTRUMENTATION LINE VOLTAGE REGULATOR

A Sorensen model 2501, 2500 va, rack-mounted regulator unit supplies regulated power to the detector high voltage power supply, the differential amplifier, and the X-Y recorder. Regulation accuracy is ±0.01% for input voltage variation of ±10%. The time constant for 63% recovery from maximum input voltage variation is 0.2 sec. Output voltage is adjustable from 110 to 120 vac.

F. DETECTOR POWER SUPPLY

The detector high voltage power supply, common to both detectors, is a John Fluke Model 412-A. Output polarity can be either positive or negative and is adjustable from 500 to 2010 v at a maximum current of 15 ma. The power supply is normally operated at about 750 vdc at an output current of about 2.5 ma. Output voltage stability is 0.005%/hr and 0.05% day.

G. DIFFERENTIAL AMPLIFIER

The differential amplifier is a Kintel model 114A with floating input and output. Gain is adjustable from 10 to 1000 in five steps. Stability is 5 v for 40 hr referred to the input. Bandwidth is 100 cps and output is 10 v at 10 ma maximum.

H. X-Y RECORDER

The X-Y recorder is a Moseley model 3S "Autograf" 2-axis graphic recorder which will accept dc signal information from related sources and automatically produce representative cartesian coordinate curves on standard 8-1/2 x 11-in. graph paper. Normally the Y axis is used to record void fraction signals from the differential amplifier and the X axis is used as a time base.

The recording mechanism employs a "drafting machine" type linkage, cable driven by independent servo motors which effectively convey Y-motion without cross-coupling to X axis. Electrically isolated high gain amplifiers control the servo motors. Input ranges are in eleven calibrate steps from 5 mv to 500 v on each axis. By means of a transfer switch, each input range may be expanded and made continuously variable to permit the fitting of arbitrary voltage to any desired scale. The recorder also contains full range zero set and one full scale length of zero suppression on each axis. These features permit full scale recording resolution of any portion of the void fraction spectrum.

Recording accuracy is better than ±0.25% of full scale and resetability is ±0.1% of full scale. The maximum recording speed is 0.5 sec for full scale travel on each axis.

I. SCINTILLATION DETECTORS

The scintillation detectors originally consisted of an NaI (Tl) crystal which is optically coupled through a polished lucite light pipe to a 6362-multiplier phototube. The crystal, light pipe, and phototube are encased by a water-cooled, light tight shield.

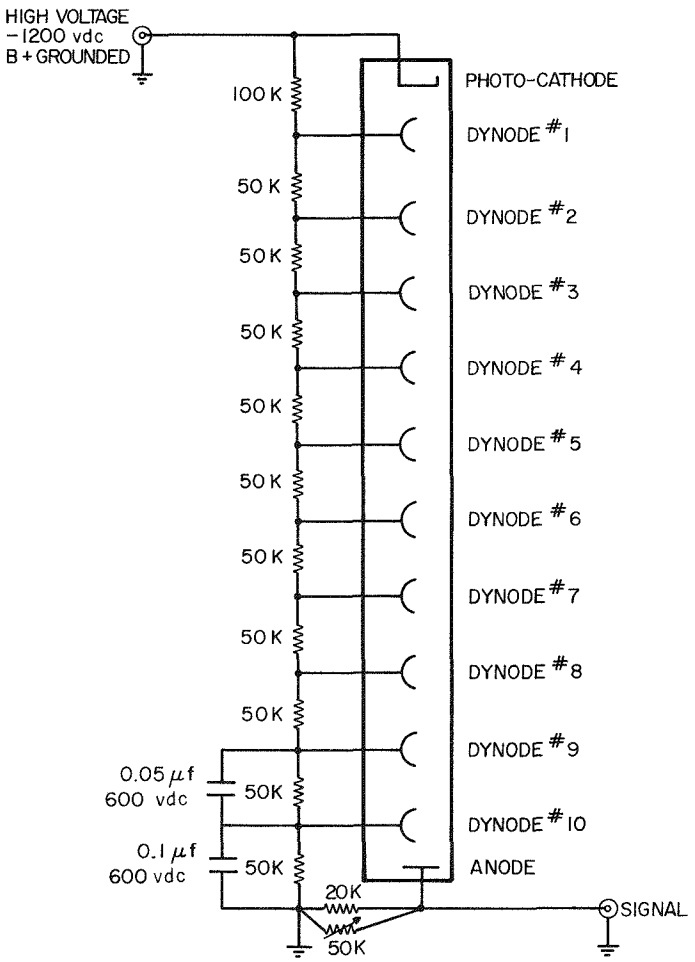

Figure 8. Scintillation Detector Schematic

The DuMont type 6362 is a 10-stage multiplier phototube with a flat end-window type photo-cathode having an S-11 response. The tube diameter is 3/4 in. and its length is 4-7/8 in. The dynode string was designed for 1200 v operation at a current of 2 ma. The scintillation detector schematic is shown in Figure 8 and the detector assembly in Figure 9.

A sodium iodide (thallium-activated) crystal of 3/4 in. diameter and 3/4 in. length is used for conversion of x-ray photons. The crystal, which is designed for low energy gamma detection, is backed with a 0.001 in. thick aluminum foil window.*

An optically polished lucite light pipe couples the scintillation crystal to the phototube. For good optical coupling, Dow-Corning DC-200 silicone oil is used to connect the crystal to the light pipe and the light pipe to the phototube. Under ideal conditions it would be best to couple the crystal directly to the phototube; however, the magnetic field generated by the test section heating current is so strong that the phototube had to be located some distance from the crystal. Magnetic field intensity at the crystal was calculated to be 96 gauss for a test section

*While calibrating the void fraction detector it was discovered that the detector output did not faithfully follow a large (50%) step change in radiation intensity such as might occur during a bubble slug measurement. The detector output would show a step change to about 98% of the final voltage level and then a leveling off period of about 5 sec for the last 2%. This caused no problem during steady state boiling measurements but could cause measurement errors of about 2 to 4% void during rapid boiling transients. In sodium iodide (NaI) crystals, this leveling off period occurs because of phosphorescence which is caused by electron trapping at energy levels associated with impurity atoms. These metastable states have been observed to last for over 30 sec in high radiation fields. The phosphorescence problem was solved by replacing the sodium iodide crystals and light pipes with a plastic scintillant of high purity and short decay constant (4×10^{-6} sec). This scintillant is known as "Polyfluor" and was obtained from Semi-Elements Inc. of Saxonburg, Pa. Although the conversion efficiency of "Polyfluor" is only about 30% of that for NaI *(Tl)*, there was sufficient beam intensity reserve capability in the x-ray generator to permit operation of the detectors at the same output level as for NaI *(Tl)*.

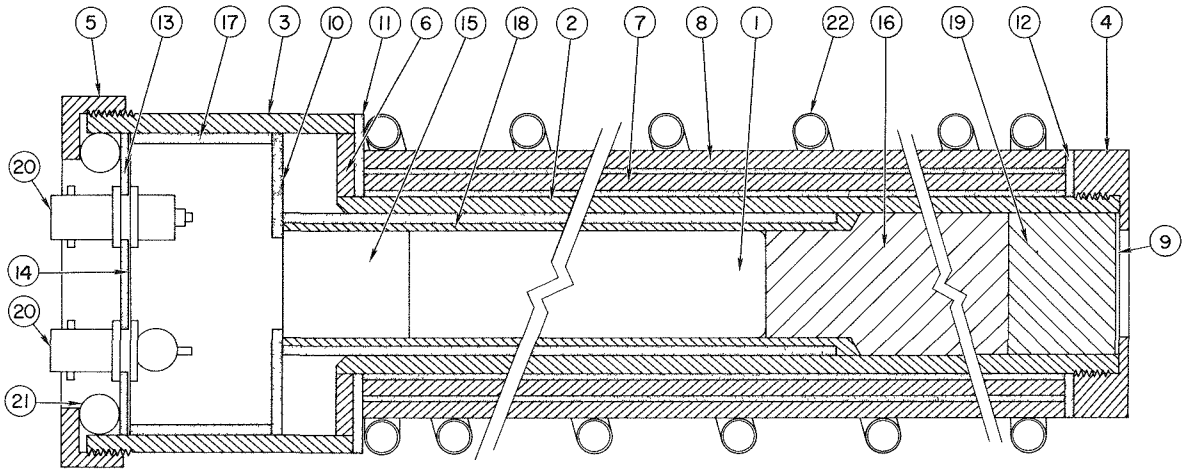

PART NO	NAME	MATERIAL
1	PHOTOMULTIPLIER TUBE	———
2	DETECTOR HOUSING	STEEL
3	DETECTOR HOUSING	STEEL
4	END CAP	STEEL
5	END CAP	STEEL
6	DETECTOR HOUSING	STEEL
7	MAGNETIC SHIELD	SOFT IRON
8	MAGNETIC SHIELD	SOFT IRON
9	LIGHT SEAL	ALUMINUM
10	INSULATING RING	POLYSTYRENE
11	INSULATING RING	POLYSTYRENE

PART NO	NAME	MATERIAL
12	INSULATING RING	POLYSTYRENE
13	INSULATING RING	POLYSTYRENE
14	RECEPTACLE SUPPORT	ALUMINUM
15	TUBE SOCKET	———
16	LIGHT PIPE	LUCITE
17	INSULATING COLLAR	POLYSTYRENE
18	MAGNETIC SHIELD	μ METAL
19	SCINTILLATION CRYSTAL	SODIUM IODIDE
20	COAXIAL CABLE RECEPTACLE	———
21	O-RING	NEOPRENE
22	COOLING COILS	COPPER

Figure 9. Detector Assembly

heating current of 2400 amp. At the photo-cathode the magnetic intensity would be a maximum of 24 gauss if shielding were not used.

Magnetic fields are attenuated by a factor of 1000 by the detector case which serves as a high intensity magnetic shield. The case consists of three concentric tubes, of 1/8-in.-thick soft iron, which are electrically insulated from each other by polystyrene tubes. During calibration we found that magnetic defocusing of the photomultipliers was not completely eliminated by the magnetic shielding. This problem was solved by wrapping a few turns of high magnetic permeability foil around the photomultiplier. Magnetic shielding also had to be applied to the x-ray tube to prevent signal changes when the current through the test section was changed.

Cooling water is circulated through a coil of 1/4-in-diameter copper tubing which is brazed to the detector case. Cooling of the detectors substantially reduces temperature induced sources of measurement error. The reduction in measurement error has been observed but not measured.

During void fraction measurement, at zero void conditions, both the reference and test section detectors deliver a dc output signal to the input of the differential amplifier. The detectors are differentially connected to the amplifier so that the resultant input signal is zero v. Since detector characteristics change somewhat with time, the detector output signals are periodically balanced by means of adjustable 50,000 ohm potentiometers which are connected in parallel with the anode load resistor. At 100% void the reference detector output remains constant, and the test section detector output increases. Differential connection of the two detectors, with almost identical output characteristics, greatly reduced measurement errors caused by variation of detector high voltage and x-ray tube output. During calibration of the void fraction detector, an attempt to measure void fraction with one detector could not be accomplished because of excessive fluctuation of detector output.

III. CALIBRATION & TESTING*

A. DETECTION SYSTEM RESPONSE TO VOID FRACTION CHANGES

The attenuation of a collimated beam of monochromatic gamma- or x-radiation as it passes through a material can be calculated from the equation

$$I = I_o e^{-\mu x} \qquad \ldots(1)$$

where

I = intensity of the radiation at a given point after passing through the material,

I_o = intensity of the radiation at the same point without the absorbing material,

μ = linear absorption coefficient of the material, and

x = thickness of the material.

Although the output of an x-ray generator is not monochromatic, the linear absorption coefficient observed experimentally for small changes in absorption is equal to that for a monochromatic source having an energy called the "effective kilovoltage" of the x-ray source. In the present case, with the x-ray generator operating at 150 kv and with the inherent filtration of the x-ray tube plus that of the nickel test section, a reasonable estimate for the effective kilovoltage is 100.

If more than one material is absorbing radiation from the collimated beam, the exponent of e becomes

$$-\sum_i \mu_i x_i \quad ,$$

where x_i is the thickness of the i^{th} material and μ_i is the corresponding absorption coefficient.

The radiation reaching the detector can be expressed by

*References 28 through 38 furnished information useful in Section III calculations.

$$I = I_o \exp\left(-\sum_i \mu_i x_i\right) \exp\left[-\mu x(1 - \alpha)\right] \quad \ldots (2)$$

where

$\exp\left(-\sum_i \mu_i x_i\right)$ accounts for the absorption of the nickel walls of the test section, the insulation around it, and the air between source and detector,

μ = linear absorption coefficient of the Santowax R,

x = thickness of the Santowax R, and

α = void fraction, the variable to be measured.

The absorption of the nickel, air, and insulation is assumed to be constant. Differentiating with respect to α gives the following equation:

$$\frac{dI}{I} = \mu x d\alpha \quad . \quad \ldots (3)$$

Substitution in this equation of 0.5 in. for the Santowax thickness and μ calculated from values tabulated in Reference 27 for 100 kv and for a density of 0.8 g/cc gives

$$\frac{dI}{I} = 0.17\ d\alpha \quad . \quad \ldots (4)$$

A consequence of this relation is that the measurement system must have good stability. For void fraction accuracy of ±5%, the measurement system stability must be about ±1%.

B. DETERMINATION OF DETECTOR OUTPUT

One r/hr corresponds to about 6×10^6 photon/cm^2-sec at 10^5 ev. The number of photoelectrons, P, which are produced at the cathode of the photomultiplier tube, due to absorption of x-radiation energy, E_p, in the scintillator, is given by the equation:

$$P = \frac{E_p \eta g}{h\nu} = \frac{E_p}{f} \quad , \qquad \ldots (5)$$

where

$f = h\nu/\eta g$,

E_p = energy absorbed in scintillator in units of thousand of electron volts,

η = the intrinsic efficiency of the scintillator, which is defined as the ratio of the light energy emitted to the kinetic energy of the absorbed particle,

$h\nu$ = the energy of the luminescent quantum, energy per photon, in units of electron volts,

g = the light efficiency of the optical system and photocathode, and is given as photoelectrons/fluorescent photon.

The figure of merit of the scintillation detector, f, is the average energy absorbed in the scintillator for each photoelectron ejected from the cathods of the photomultiplier.

For a scintillation detector with good optical and geometrical light utilization, the figure of merit, f, is approximately $2/\eta^*$, where η^* is the light yield with reference to anthracene. For NaI(Tl), η^* is 2. Therefore for this case the figure of merit, f, is equal to 1. $P = E_p/f = 100/1 = 100$ electron/photon. One electron/sec corresponds to 1.6×10^{-19} amp. The collimator area is 0.322 cm^2.

Assuming all the photons entering the scintillator are absorbed, the photocathode current may be calculated as follows:

$$I_{cathode} = P\left(\frac{\text{electrons}}{\text{photon}}\right) \times 6 \times 10^6 \left(\frac{\text{photons/cm}^2\text{-sec}}{\text{r/hr}}\right) \times 1.6 \times 10^{-19} \left(\frac{\text{amp-sec}}{\text{electron}}\right) \times 0.322 (\text{cm}^2)$$

$$= 3.1 \times 10^{-11} \left(\frac{\text{amp}}{\text{r/hr}}\right) \quad . \qquad \ldots (6)$$

If the photomultipliers are operated at a gain of 1.5×10^5, the output current is:

$$I_o = I_{cathode} \times \text{gain} = 3.1 \times 10^{-11} \times 1.5 \times 10^5 \simeq 5 \times 10^{-6} \frac{\text{amp}}{\text{r/hr}} \qquad \ldots (7)$$

The maximum output of the x-ray generator is 3.8×10^7 r/hr at a target-to-specimen distance of 1 in. The radiation will be attenuated by the test section, coolant, air, and insulation. Even with the inverse square law correction and a large correction for absorption, the photomultiplier currents will be orders of magnitude above the dark currents. Therefore, both the x-ray generator and the photomultipliers can be operated at well below their maximum rated levels.

C. STATISTICAL ERROR

To avoid photomultiplier fatigue effects, it is desirable to operate them in a system such as this at levels well below the maximum rated level. The output currents would then be in the microampere region. According to the calculation in the previous section, assuming the photomultiplier gain is reduced to 1.5×10^4 and I_o should be 50 μa, the radiation level after penetrating the test section would be about 100 r/hr. At 100,000 ev, this would correspond to about 6×10^8 photon/cm^2-sec. Of these, 1.9×10^8 would enter the detector per sec.

Assuming a measurement system time constant of 0.01 sec, 1.9×10^6 photons would enter the detector.

Since the circuit is a ratemeter type, the relative standard deviation is given by the following:

$$\sigma = \frac{1}{\sqrt{2 \times 1.9 \times 10^6}} = 5.1 \times 10^{-4} \qquad \ldots(8)$$

Therefore, statistical variations should not be a large source of error. Statistical variations could be reduced by increasing the x-ray generator output and decreasing the photomultiplier gain.

D. CALIBRATION OF THE SYSTEM

The void fraction measuring system is calibrated by inserting a 0.122-in. aluminum block into the x-ray beam being transmitted through the reference test section. This calibration is normally done before and after each run. The aluminum block was calibrated by comparing the recorder deflection obtained when the aluminum block was inserted to that deflection obtained when the test section changes from 0 to 100% void. Due to the differential nature of the signal being recorded, inserting the aluminum block in the dummy channel

produced a signal of the same polarity as that obtained when voids are produced in the test section. Several calibrations of the aluminum block produced an average deflection of 78% of that obtained for 100% void after the figures were adjusted to represent Santowax R at 700°F.

Signal strength adjustment in either the reference or test section channel is accomplished by adjustment of a 50-k ohm potentiometer in parallel with the 20-k ohm anode resistor. Normal procedure is to adjust the 50-k ohm potentiometers, immediately before a boiling run is to be made, so as to obtain a differential output of zero. The solenoid which inserts the aluminum calibration block is then remotely actuated from the control panel. The calibration deflection thus obtained may be expanded or contracted by adjusting the recorder gain, differential amplifier gain or the detector power supply voltage. Immediately following the boiling run, a calibration deflection is again obtained to insure that nothing has happened which would cause the gain of the system to vary.

E. DATA REDUCTION

Figure 10 represents a typical recording of a calibration and a void fraction signal. The void fraction (α) at the point V is determined as follows. A point Z is marked on the trace at a point where it is known that no voids exist ($\alpha = 0$). The average bulk temperature of the Santowax (T_z) at the point Z is available from another trace which is being recorded simultaneously. The average bulk temperature at the point V, (T_v), is also obtained and the equivalent void fraction represented by the density change of the Santowax R from T_z to T_v is calculated. This equivalent void fraction is given by the following formula.

$$\text{Equivalent void fraction} = -(T_v - T_z)\frac{\Delta\rho}{\Delta T}\frac{1}{\rho_{st}}, \qquad \ldots(9)$$

$\Delta\rho/\Delta T$ = rate of change of the density of Santowax R with temperature.

ρ_{st} = density of Santowax R at its saturation temperature.

The negative sign is necessary because $\Delta\rho/\Delta T$ is negative.

The total void fraction represented by a change in signal from point Z to point V is $(V - Z)/C \times E_c$ where E_c is the equivalent void fraction represented by the aluminum calibration block. Subtracting the equivalent void fraction represented by the density change from T_z to T_v we obtain:

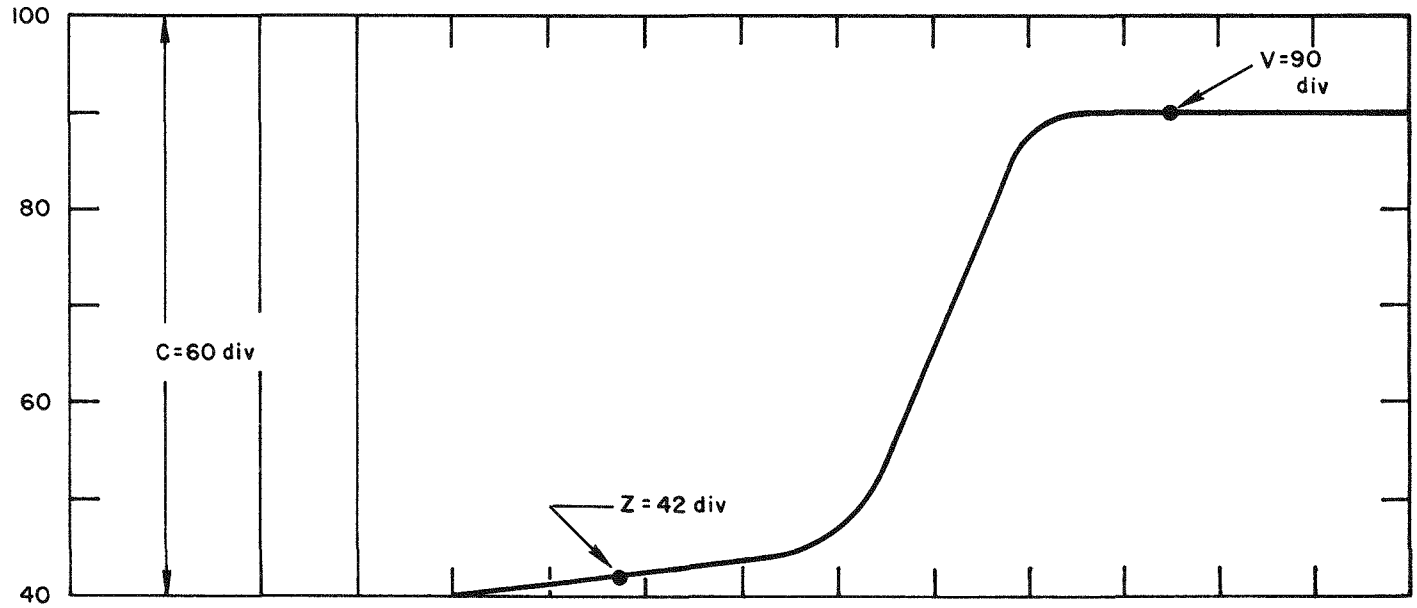

Figure 10. Typical Void Fraction Signal vs Time

$$\alpha = \left(\frac{V - Z}{C}\right) Ec + (T_v - T_z)\frac{\Delta\rho}{\Delta T}\frac{1}{\rho_{st}} \quad . \qquad \ldots(10)$$

This equation may also be written

$$\alpha = \left(\frac{V - Z}{C}\right) 0.78 \left[1 + 5.7 \times 10^{-4}(T_s - 700)\right] + \left[(T_s - T_z)\frac{\Delta\rho}{\Delta T}\frac{1}{\rho_{st}}\right] \quad . \qquad \ldots(11)$$

This equation is correct, assuming that we have a straight line correlation between % deflection and % void fraction (% deflection = % void fraction).

$$\text{Actually, \% deflection} = \%D = 100\,\frac{\epsilon^{0.1595\alpha} - 1}{\epsilon^{0.1595} - 1} \quad .$$

This curve is shown in Figure 11.

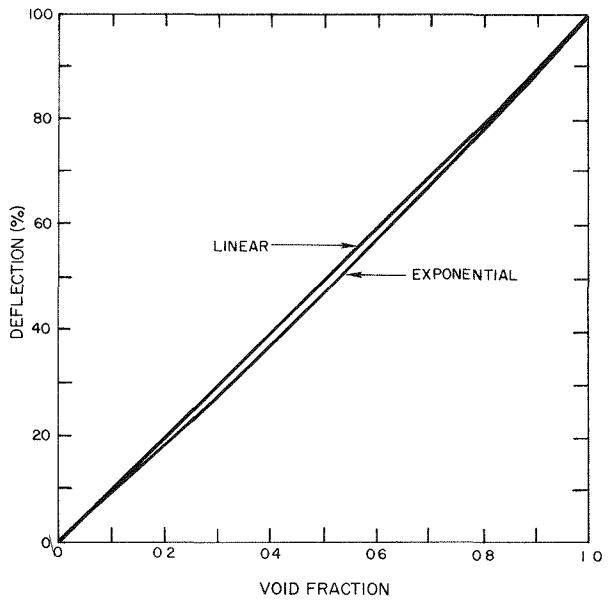

Figure 11. Void Fraction vs Relative Deflection, Assuming Both Linear and Exponential Function

$$\alpha = \frac{1}{0.1595} \ln (1 + 0.173D)$$

$$\% \text{ void error} = 100\left[D - \frac{1}{0.1595} \ln (1 + 0.173D)\right]$$

$$\% \text{ error} = 100\left[\frac{0.1595 - \ln (1 + 0.173D)}{\ln (1 + 0.173D)}\right] . \qquad \ldots (12)$$

These two curves are plotted in Figure 12. It is seen that the error can be approximated by a straight line with end points of 7.85% error at 0% deflection and 0% error at 100% deflection.

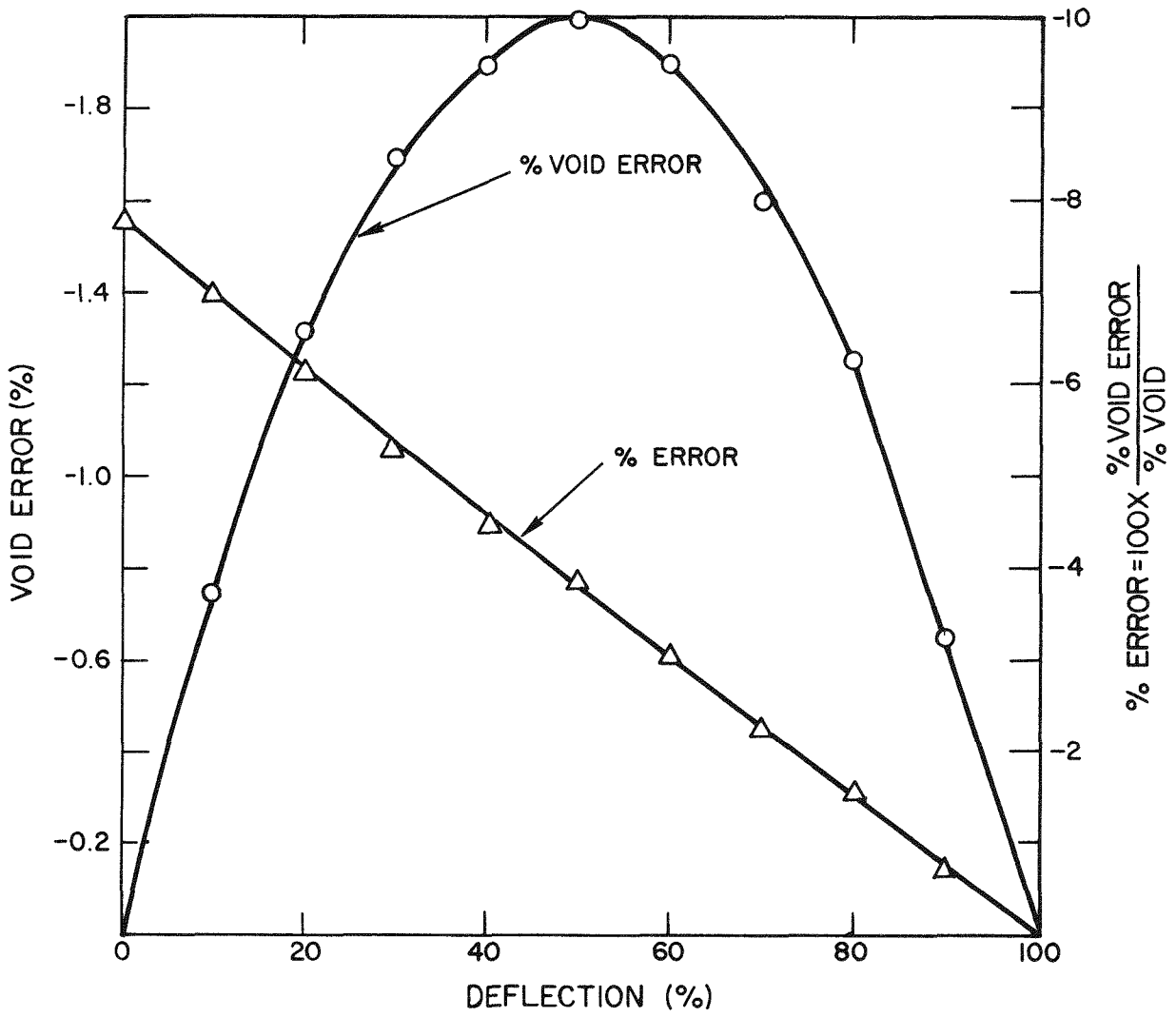

Figure 12. Error Introduced by Assuming Void Fraction Signal is Linear Function of Void Fraction

F. HORIZONTAL POSITIONING OF THE VOID FRACTION DETECTION SYSTEM

Several variables are plotted in Figure 13. Curves A and B are plots of the relative strength of the attenuated beam vs horizontal position. These curves assume a beam of zero width. Curves C and D are the same except that a beam with a width of 0.0958 in. is assumed. This is approximately the width of the beam which is used. Curve E is a plot of the difference in magnitude of the 100% void signal and the 0% void signal, referred to the center line of the test section. Curve E was obtained from Curves A and B. A similar curve obtained from Curves C and D would be identical except for points close to the wall of the test section. Curve E shows that the horizontal positioning of the x-ray beam (about the center line of the test section) is not a critical factor. A beam which is "off center" by as much as 10 mils will cause less than 1/2% change in the 0 to 100% void signal.

G. THEORETICAL VERIFICATION OF THE VOID EQUIVALENCE OF A 0.122-IN. ALUMINUM BLOCK

When determining the attenuation coefficients of a compound like Santowax R, the attenuation coefficients of the elements contained are weighted according to their percentage by weight in the compound. The attenuation constants for 0.4785 in. of Santowax R (6.1% hydrogen, 93.9% carbon) and 0.122 in. of aluminum are plotted in Figure 14 for several values of kilovoltage.

The 0.122-in. aluminum block was inserted into the x-ray beam of the reference channel and the resulting signal reduction enabled us to calculate the attenuation constant "K_{Al}" of the aluminum. The attenuation constant for 0.4785 in. of Santowax R (K_s) at 700°F was then determined from Figure 14. The change in signal produced by the calibration is negative and equal in magnitude to $C(\epsilon^{-K_{Al}} - 1)$, where C is a constant determined by the gain of the system. The change in signal resulting from production of 100% voids is positive and equal in magnitude to $C(\epsilon^{K_s} - 1)$. The ratio of the magnitude of these two signals is equal to the % void represented by the calibration if we assume a linear relationship between void fraction and signal. This assumption is not strictly true due to the exponential nature of the signal. The error is small, however, and may be accounted for in the data reduction procedure if the increase in accuracy is desired.

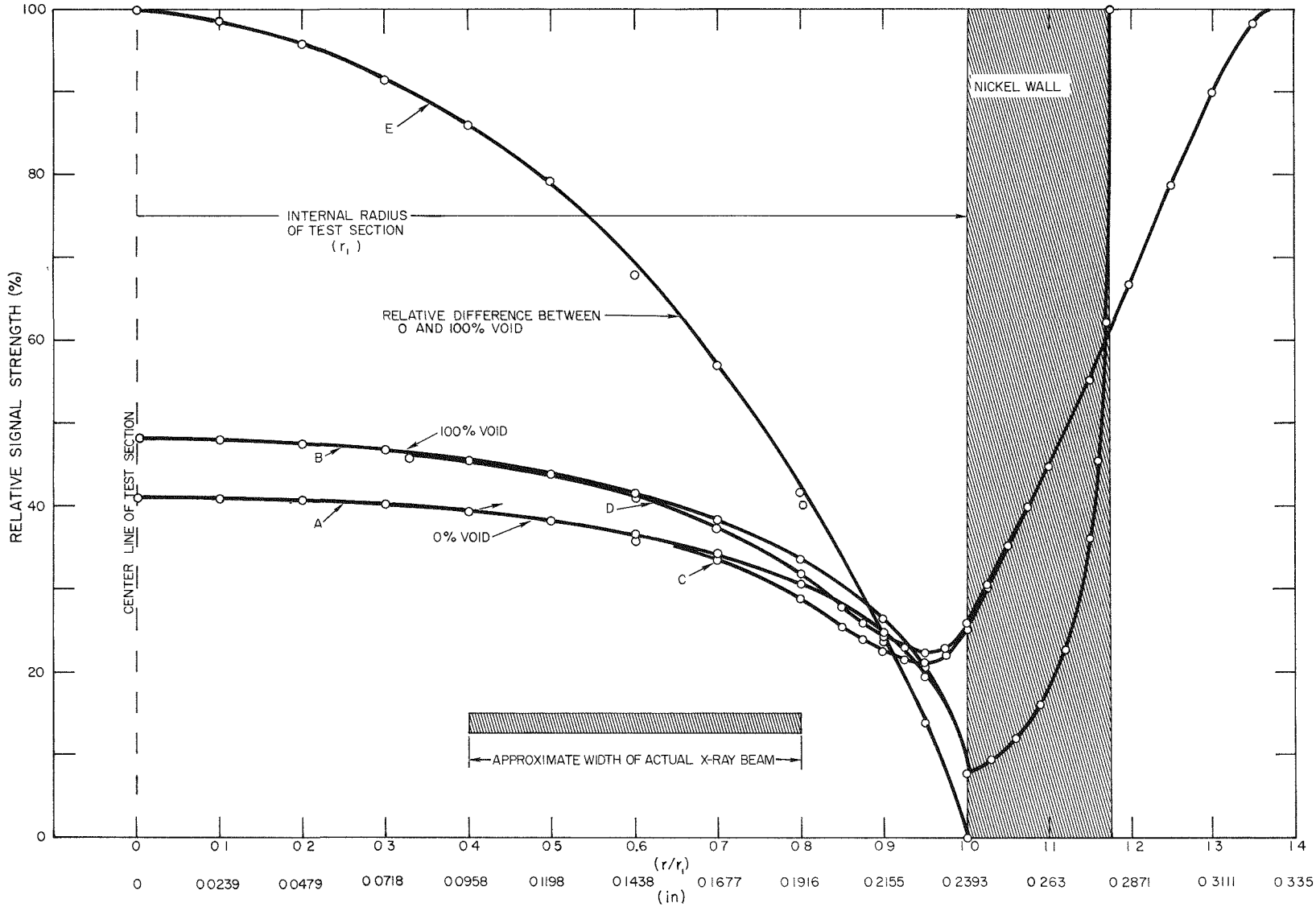

Figure 13. Relative Signal Strength for Horizontal Scan of Test Section for 108-kev Beam

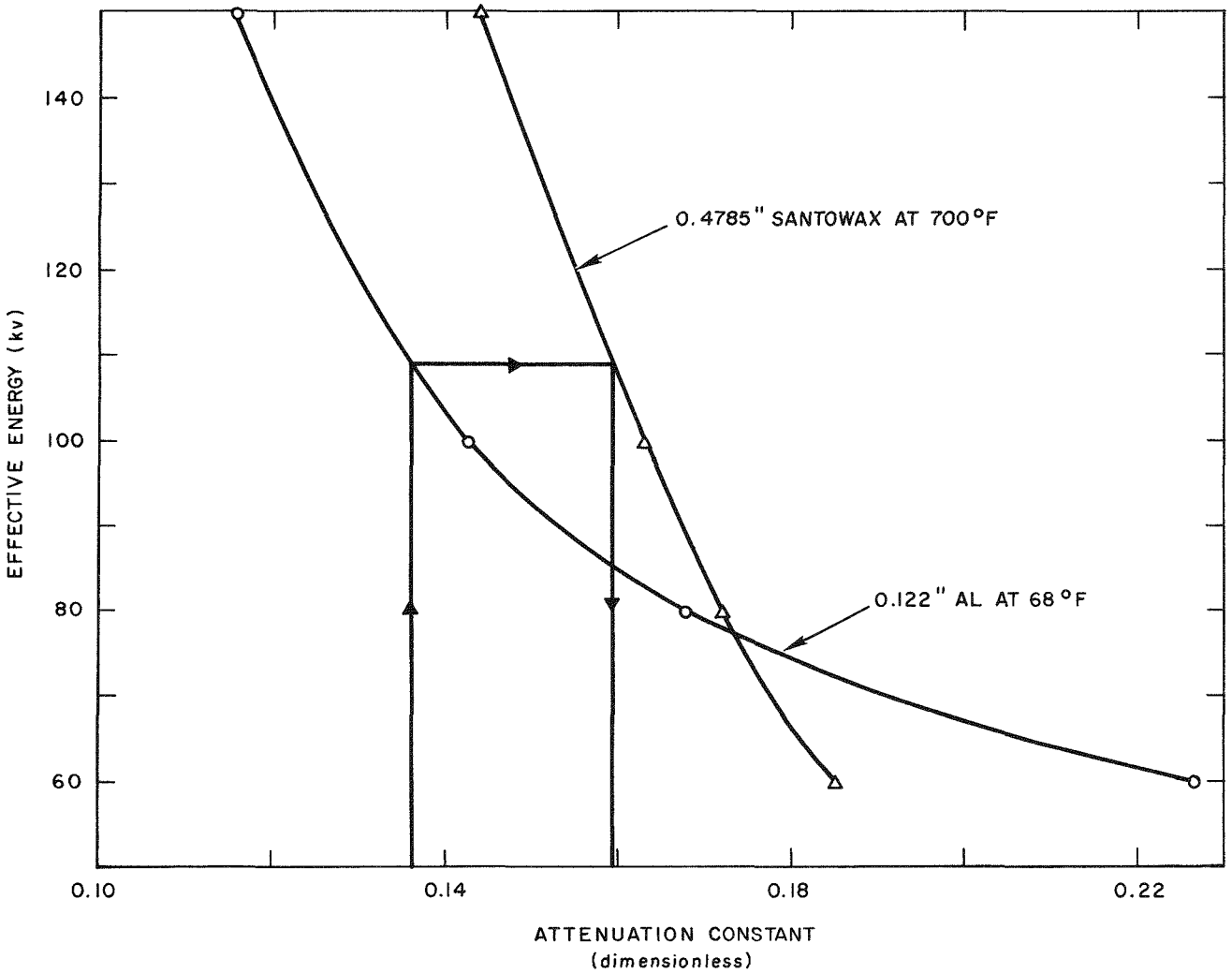

Figure 14. Attenuation Constants for Al and Santowax vs Effective kv

Figure 15 is a plot of the void fraction represented by the 0.122-in. aluminum calibration block vs $\epsilon^{-K_{Al}}$. Indirectly, this graph is a plot of the void fraction represented by the aluminum block vs the effective kilovoltage seen by the block and the Santowax.

The measured value of $\epsilon^{-K_{Al}}$ was 0.873 as shown on Figure 15. This predicts that the deflection produced by the calibration block will be 73.6% of that produced by 100% voids. The calibration block actually produces a deflection of 78% of that produced by 100% voids, a difference of 4.4% void. There are several possible sources for this error. If we take the derivative of $E_c = (1 - \epsilon^{-K_{Al}})(\epsilon^{K_s} - 1)^{-1}$ with respect to its variables we can calculate the magnitude of the effect of errors in the various parameters.

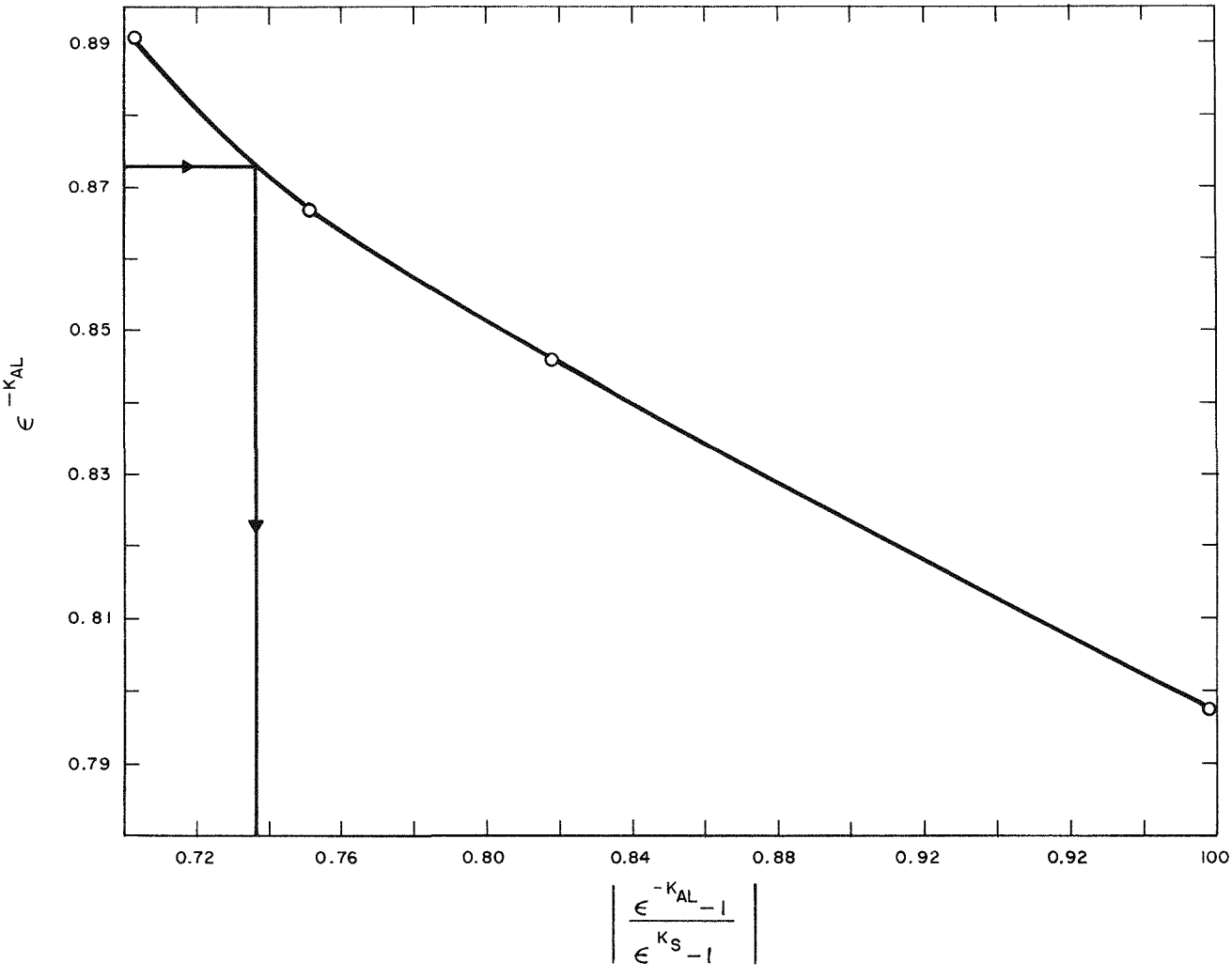

Figure 15. Graph for Determining Effective Void Fraction Worth of Aluminum Calibration Block

$$\frac{\partial E_v}{\partial K_{Al}} = (\epsilon^{K_s} - 1)^{-1} \cong 5.8$$

$$\frac{\partial E_v}{\partial K_s} = (\epsilon^{-K_{Al}} - 1)\epsilon^{K_s} (\epsilon^{K_s} - 1)^{-2} \cong 5$$

$$\frac{\partial E_v}{\partial (\epsilon^{-K_{Al}})} = - (\epsilon^{K_s} - 1)^{-1} + (1 - \epsilon^{K_{Al}})(\epsilon^{K_s} - 1)^{-2} \epsilon^{K_s} \epsilon^{K_{Al}} \frac{\partial K_s}{\partial K_{Al}} \cong -2.3 \quad \ldots (13)$$

K_{Al} and K_s are accurate to 3%, and $\epsilon^{-K_{Al}}$ shall be assumed to have been measured accurately to within 1%. The maximum possible error in E_v from these sources would be

$$\left|dE_v\right| = 5.8dK_{Al} + 5dK_s + 2.3d(\epsilon^{-K_{Al}})$$

$$= 5.8 \times 4 \times 10^{-3} + 5 \times 4.8 \times 10^{-3} + 2.3 \times 8.7 \times 10^{-3}$$

$$= 0.067 = 6.7\% \text{ void} \quad . \qquad \ldots(14)$$

H. ACCURACY OF VOID FRACTION MEASUREMENTS

The void fraction Equation No. 10 is repeated below.

$$\alpha = (V - Z)\frac{E_c}{C} + (T_v - T_z)\frac{\Delta\rho}{\Delta T}\frac{1}{\rho_{st}} \quad .$$

It is necessary to examine each term of this equation to determine the accuracy of the measurement. E_c/C determines the % void/division on the recording. For a typical run, C is adjusted to span approximately 80 divisions. The recorder may be read to within 0.3 division, which gives an accuracy of 0.3% (C = 78% void). By the same type of analysis, E_c is determined to be accurate to within 0.3%. This gives an accuracy of 0.6% for the term E_c/C.

Using the same reasoning (V - Z) may be read to within 0.3 divisions. This, however, does not represent 0.3% error, but 0.3% void error. Looking at the second term of the equation, $\Delta\rho/\Delta T$ and $1/\rho_{st}$ are both accurate to within 0.1%, and $(T_v - T_z)$ is accurate to within 1%. This gives an accuracy of 1.2% for the second term. For practically all runs the second term is less than 10% void, which means that the accuracy of the term is better than 0.12% void.

Figure 16 shows a typical signal drift curve from the moment the x-ray generator is turned on. If the x-ray generator is allowed to warm up at least 2 hr and the drift is measured at least every hour, the deviation of the drift curve from a straight line extrapolation will be less than 1% void.

The differential amplifier and the recorder are both linear to within 0.1%, and the linearity of the photomultiplier tubes and crystals is assumed to be perfect.

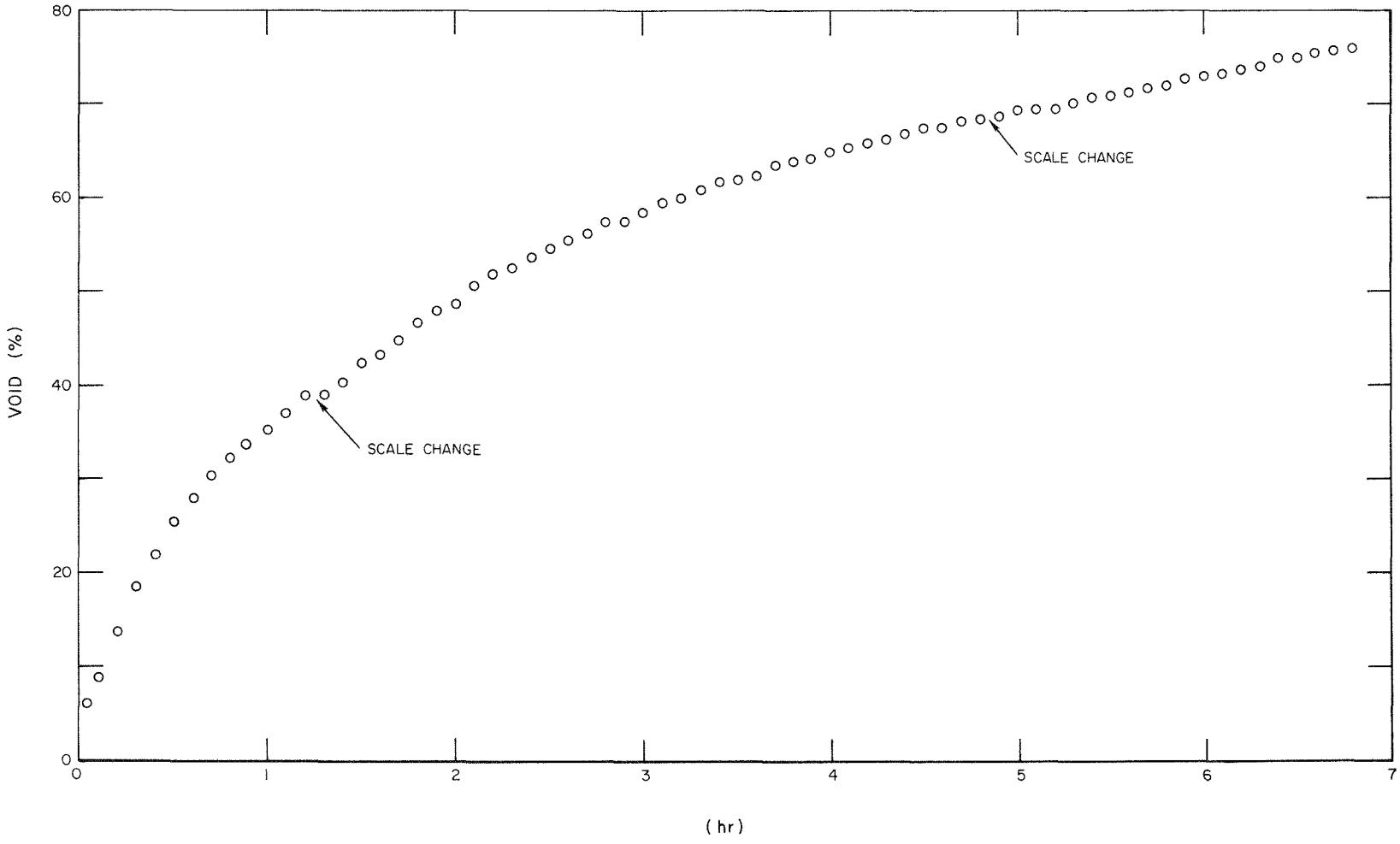

Figure 16. Typical Drift of Void Fraction Signal vs Time

The various sources of error are all listed below and are separated into two groups. Group I contains errors which are percentages of the signal being measured while Group II contains fixed void fraction errors.

I		II	
E_c/C	0.6	$(T_v - T_z)$	0.1
Amplifier	0.1	$1/\rho_{st}$	0.01
Recorder	0.1	$\Delta\rho/\Delta T$	0.01
Total error	0.8%	Drift	1.0
		V - C	0.3
		Total error	1.42% Void

The total effect in % error vs void fraction is plotted in Figure 17.

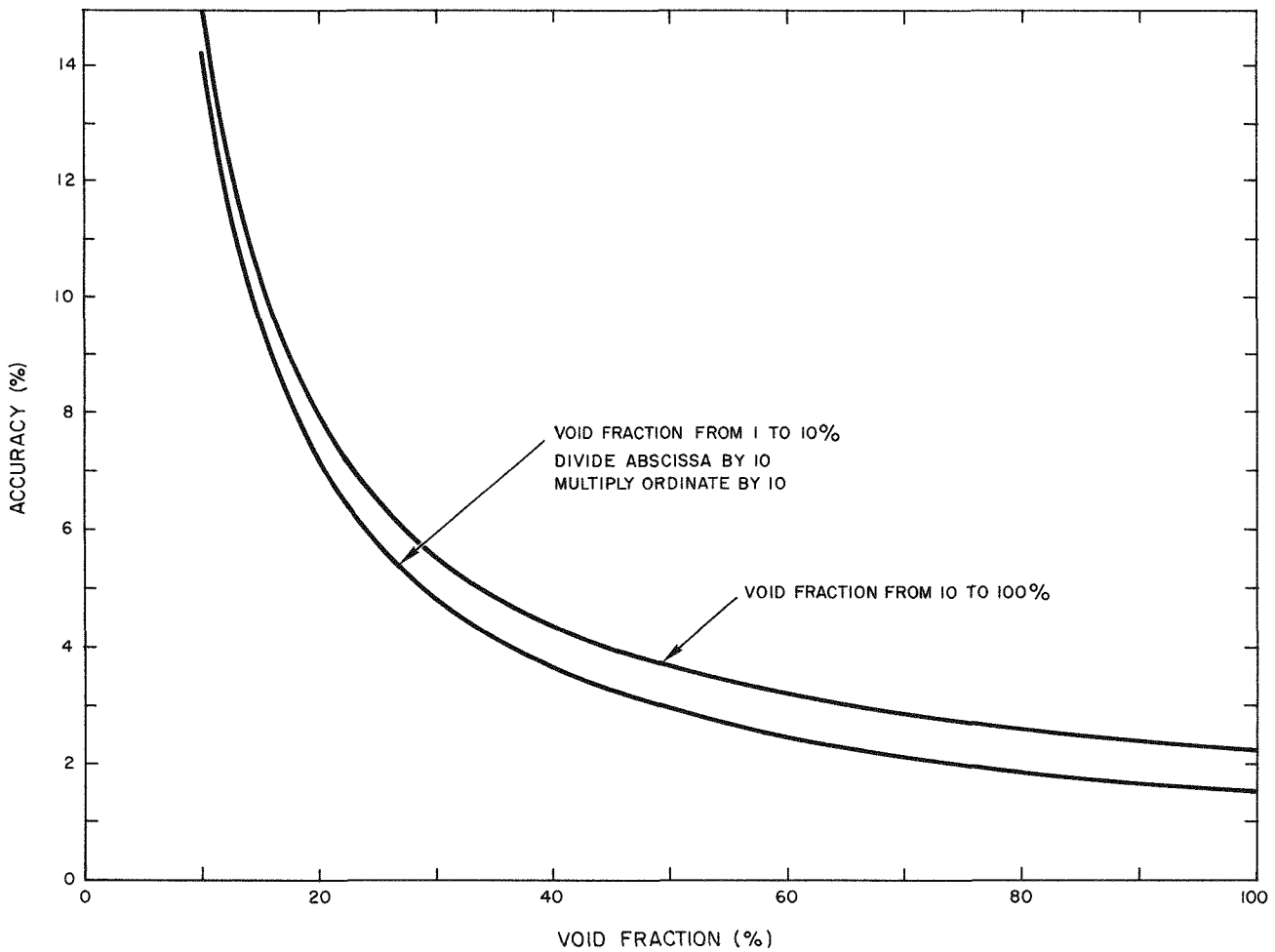

Figure 17. Void Fraction Measurement Accuracy

I. TRANSIENT MEASUREMENTS

The ability to make transient measurements in any instrumentation system is limited by those components having the smallest bandwidth. In this system, the differential amplifier and the recording galvanometer are the limiting factors, each with a high frequency cutoff of 100 cps and a low frequency cutoff of 0 cps. Any transient which has the major portion of its power spectrum in the 0 to 100 cps range will be faithfully reproduced.

Looking at the response of a system to a pulse input imports valuable insight to its transient characteristics. If a pulse is applied to a system with a cutoff frequency f_c, the pulse width τ should be equal or greater than $5/f_c$ if the output is to closely resemble the input. For this system, the pulse width should be $\tau = 5/100 = 0.05$ sec. The rise time of the output pulse would be $0.8/100 = 0.008$ sec or $0.5/100 = 0.005$ sec, depending upon the definition of rise time. The transient response of the system will therefore permit faithful measurement of boiling transients with a rise time of 5 msec or longer and a duration of 50 msec or longer.

APPENDIX

LITERATURE SURVEY OF VOID FRACTION DETECTION METHODS

A. EXTENT OF SURVEY

The literature search on methods of void-fraction measurements covers the period from 1951 to date and includes work done in England, Germany, and New Zealand, as well as in the U.S.A. Forty references are listed in the bibliography. Of these, 21 have been reviewed; and of those reviewed, 18 are abstracted in Table I. Those references reviewed but not abstracted in Table I duplicate information already in this table. References 1, 9, 18, 20, 21, and 26 were not available for review, but the information contained in those references would not change the conclusions of this literature survey.

Table I summarizes results of previously published attempts to measure void-fraction in various types of 2-phase flow systems. The references are entered in chronological order.

It is immediately apparent from Table I that the most commonly used method of measuring void-fraction is by means of γ-ray attenuation (14 references) and the least used method is that of a radioactive tracer (1 reference). Gamma-ray attenuation has been tried by investigators at Tulane,[3] Battelle Memorial Institute,[1] University of Minnesota,[7] MIT,[12] and principally at Argonne National Laboratory.[2, 4,5,6,10,11,13,14] Photographic techniques have been used at MIT[25] and the Jet Propulsion Lab[24] while x-ray attenuation has been tried at the University of California,[15, 16] the General Electric Company,[17] and currently at Ramo-Wooldridge.[18] Beta particle absorption has been used at the General Electric Company,[20] the University of Washington,[23] in New Zealand,[21] and in England.[22]

On the basis of void-fractions actually reported as measured, it appears that the various methods in order of decreasing sensitivity are: photographic, x-ray attenuation, β-absorption, γ-attenuation, and radioactive tracer. It is not possible to determine what the actual accuracies were in most of the reviewed references.

B. DISCUSSION OF PUBLISHED RESULTS ACCORDING TO METHOD

1. Photographic

The use of high-speed photography is perhaps the most informative and most sensitive method of measuring void-fraction. However, the process of taking high-speed photographs and then counting and measuring bubbles is tedious and time-consuming. The successful use of a visual method is limited to an apparatus with some transparent wall area, usually glass. The use of glass imposes serious limits on the allowable operating temperature and pressure levels. Finally, the methods can be accurately employed only in low void-fraction situation; i.e., 0.2 or less, because of the difficulty encountered in interpreting 2-dimensional photographs of a 3-dimensional phenomenon.

In spite of the difficulties mentioned above, Griffith[25] measured void-fraction as low as 0.0002. Gunther[24] did not actually measure void-fractions, but such information can be extracted from his data. Much of the analytical work in the literature is based on these two visual studies as they have provided the analyst with a model of the flow phenomena investigated; namely, forced convection nucleate boiling.

2. γ-Ray Attenuation

The most commonly used source of γ-rays has been the 0.084 mev peak of thulium^{170}* with selenium^{75}† and iridium,^{192}§ each being used once. All investigators have used thallium-activated NaI scintillation crystals in conjunction with some type of photomultiplier tube as a detector system. Various source geometries and types of source collimation have been tried. Best results were obtained when a well-collimated beam of γ-radiation was employed.

The lowest void fraction actually reported as measured (but with unknown accuracy) is 0.01 by Richardson.[14]

3. X-Ray Attenuation

In principle, the x-ray attenuation method is identical to the γ-ray attenuation method, the only differences being the nature of the source of photons and their relative energy, x-rays generally being a softer radiation. An x-ray system is identical to a γ-ray system with the additional complication that the x-ray

*References 1, 2, 4 - 6, and 8 - 14.
†Reference 7.
§Reference 3.

tube which serves as a source of radioactive particles must be cooled. If the void-fraction measuring apparatus is to traverse the length of a test section, then flexible electrical leads and cooling water supply lines to the x-ray tube must be used.

4. β-Particle Absorption

A statistical analysis of the absorption of beta particles is complicated by the fact that they are emitted with a continuous spectrum and that a beta particle can lose a large fraction of its energy in one collision. However, it has been shown that an exponential absorption law combined with a maximum range is approximately valid.

If strontium^{90} (β energies to 2.2 mev) is used as a source, then the total weight/unit area of absorbing material between the source and detector should not exceed 1.2 gm/cm^2. This implies that only thin-walled, small-diameter tubes or thin-wall, closely spaced channels can be used as a test section.

Even though the β-absorption method is limited to use in thin cross-sections, it has the advantage that it is possible to obtain a well-defined beam for use in making measurements of void fraction.

Costello[23] has reported void-fraction of 0.03 ± 0.013 with strontium^{90} as the β-particle source. He employed an annular test section with a cylindrical source inside the inner stainless steel tube and the detector outside the outer glass tube. Water was the test medium.

5. Radioactive Tracer

Only one investigator, Dengler,[26] has reported using this technique. It is essentially a γ-ray attenuation technique with the source distributed in the test fluid. This technique offers no advantages over the previously discussed methods. Serious safety problems are introduced by the use of this method.

C. TYPE OF VOID-FRACTION MEASUREMENT

In examining Table I, one will see the following expressions: (1) One shot, (2) Local traverse, and (3) Longitudinal traverse. These expressions are defined below.

1. One Shot

At a given cross section along the length of a test section, the attenuation of a beam of radioactive particles is measured and the void-fraction inferred. In some cases, the beam dimensions are such that only a portion of the flow through the cross section of the test section is scanned. In other cases, the beam is wider than the test section, and the entire flow through the cross section is scanned.

2. Local Traverse

In this case, at a given cross section along the length of the test section, a well defined beam of radioactive particles and an equally well-collimated detector are simultaneously traversed across a cross section of the test section. In this case, the dimension of the beam of radioactive particles in the direction of traverse is much less than the corresponding dimension of the test section being scanned.

3. Longitudinal Traverse

Usually a one-shot local measurement is used here with the source and detector simultaneously traversing the length of the test section, giving information as to the distribution of void-fraction along the length of the test section.

The most informative type of measurement would be a combination of local and longitudinal traversing. This, however, would not be possible in transient situations as such a measuring procedure would be time consuming.

TABLE I

SUMMARY OF METHODS AND RESULTS OF VOID FRACTION MEASUREMENT

Reference and Date	Flow Direction and Test Fluids	Test Section Material and Geometry	Test Conditions	Source Type, Geometry, Strength, and Collimation	Detection Equipment, Beam, & Collimation	Calibration	Type of Measurements Made	Minimum Measured Void Fraction Reported
				X-Rays				
(15) 3/51	Vertical upflow of water subcooled and bulk boiling	1/4" ID x 25" long stainless steel	Pressure, 100 to 2500 psia. Subcooling, 0 to 236°F. Heat flux to 3.8×10^6 Btu/hr-ft^2. Mass flow, 0.96×10^6 to 7.7×10^6 lb/hr.	250 kv, 10 ma. Westinghouse X-ray unit	Cadmium-tungstate crystals, lucite light pipe, photo-multiplier tube	No Data	One shot	0.01 g/cc @ 0 cps 0.04 g/cc @ 100 cps
					ECA 5819 photo-multiplier calcium tungstate scintillation crystal	Full - empty readings and interpolation	One shot	0.05
(16) 10/54	No flow water - steam	Pyrex battery jar 6-1/2" x 8-1/2" x 11-1/2" electric resistance bulk heating of liquid	Pressure, 14.7 and 135 psia	Westinghouse 250,000 v Quadrocondex therapy unit operated at 10 ma. No external regulation or filtration of power supply.	Ba SO_4 screen on RCA 931A photo multiplier converted to NaI crystal and Dumont 6292 photo-multiplier.	Full - empty and interpolation	One shot sample of cross section vertical traverse.	No Data
(19) 2/29/60	Vertical upflow water - steam	1060 aluminum, 24.625" long x 0.830" x 0.116". Electrically heated	No Data	G. E. CA-7 Mo target x-ray tube in G. E. XRD-5 diffraction x-ray machine line voltage and tube current stabilization, 30 kv potential, 23 ma tube current. Converted to constant potential machine.				
				β Attenuation				
(22) 2/55	Vertical upflow of water-subcooled boiling	Rectangular channel, 0.177" x 0.80" x 60 cm. Oval channel, 0.177" x 0.80" x 60 cm. Heated length, 60 cm. Stainless steel with 0.010" wall thickness.	Exit pressure, 30" H_2O. Inlet velocity, 12'/sec. Inlet temperature, 44.3°C. Heat flux to 550 w/cm.	Praseodymium-144 and daughter cerium-144. 20 mc, 1/2" diam beam	End window Geiger tube with 2 min counting time. Ionization chamber, 1/2" diam hole in detector shield.	Full - empty with various liquids and interpolation	One shot longitudinal traverse	No Data
(23) 8/59	Vertical upflow of water-subcooled boiling	Flow in annulus, 0.190" OD. Inner heater tube, 304 stainless steel. 0.516" ID outer tube, stainless steel or glass.	Pressure, 34" Hg. Inlet velocity, 1.5, 3, and 4 fps. Heat flux to 8.21×10^5 Btu/hr-ft^2.	strontium-90 (β up to 2.2 mev) no collimation	Geiger tube and Tracerlab scaler, model SC-51	Lucite mockup with 3 different source strengths	One shot longitudinal traverse	0.03 ± 0.013
				Photographic				
(25) 8/58	Vertical upflow of water-subcooled boiling	Rectangular 2 sides glass, 1 side heater strip, 0.378" wide x 3" long. 0.5, 0.18, or 0.09" to opposite wall from heater.	Pressure, 500, 1000, 1500 psia. Water velocity, 20 and 30 fps. Heat flux, 0.25×10^6 to 2.7×10^6 Btu/ft^2.	Bubble counting and measurement	Bubble counting and measurement	None required	No Data	0.0002

TABLE I (Continued)

Reference and Date	Flow Direction and Test Fluids	Test Section Material and Geometry	Test Conditions	Source Type, Geometry, Strength, and Collimation	Detection Equipment, Beam, & Collimation	Calibration	Type of Measurements Made	Minimum Measured Void Fraction Reported
				γ-Ray Attenuation				
(2) 4/15/55	No flow only stationary lucite models and layers of water, steel, and brass	No Data	Ambient	thulium-170 No collimation	No Data	No Data	One shot of Lucite models and water-air models	Lucite model 0.136 + 60% - 100% H_2O layers 0.044 ± 15%
(3) 12/21/55	Vertical, no liquid throughput air - water air - methanol air - glycerine	2"-std steel pipe, 6-, 10-, & 20'-long. 6"-glass pipe, 10'-long. 6- & 12"-std steel pipe, 10- & 20'- long. 24"-std steel pipe, 5'-long.	Gas velocity to 5.7 fps Liquid velocity to 10 fps	iridium-192 1/2" diam beam	thallium-activated NaI crystal	Test section full and empty	Radial traverse, source inside pipe, moved along diam in 24" pipe	0.09
					Dumont photo multiplier tube, and scintillation crystal	No Data	No Data	0.05
(4) 12/55	Vertical upflow steam - water	1/4 x 4 x 60" stainless steel	Pressure, 600 psia. Mass flux, 3.10^5 lb/hr-ft^2	thulium-170 1/2 r/hr @ 1 ft	Dumont photo multiplier tube, Hewlett Packard current amplifier, and Esterline Angus recorder	Interpolation between full liquid and full vapor	One shot traverse longitudinal	0.1
(5) 2/56	Vertical upflow steam - water	5 parallel channels 2-7/32 x 3-5/8 x 48" (outer) 3-7/16 x 3-5/8 x 48" (inner) 304 stainless steel	Pressure, 114.7 to 615 psia. Inlet velocity, 1.52 to 1.83 ft/sec. Exit quality, 1.9 to 8.2%.	thulium-170 (0.085 mev γ) 1/2 r/hr @ 1 ft	Dumont photo multiplier tube, Hewlett Packard current amplifier, and Esterline Angus recorder	Lucite mockups water - air layers	One shot traverse longitudinal	0.006
(6) 11/56	Vertical upflow steam - water	7/16" x 3-11/16" x 2' 7/16" x 3-11/16" x 4' stainless steel	Pressure, 164.7 to 614.7 psia. Inlet subcooling to 20°F Exit quality to 0.15%	thulium-170 (0.085 mev γ) 2 r/hr @ 1 ft				
(7) 3/57	Vertical upflow of steam - water mixtures	0.872" ID x 16' long	Mass flow rates used 0.347, 0.526, & 0.702 lb/sec. Maximum quality 4%	selenium-75 10 μc, collimated by 1/16" diam aperture	Model DS-1, Nuclear Instrument and Chemical Corp. scintillation counter	No Data	Longitudinal traverse Local traverse Rotation around test section to sample various diam at a given station	0.1
(8) 2/57	Vertical upflow of steam - water mixtures	304 stainless steel rectangular 1 x 0.103 x 27" electrically heated	Pressure, 2000 psia. Heat flux, 0.04×10^6 to 0.50×10^6 Btu/hr-ft^2. Mass flux, 0.7×10^6 to 0.9×10^6 lb/hr-ft^2 Inlet temperature, 500, 575, and 625°F.	thulium-170 (0.085 mev and 0.053 mev peaks) collimated by 0.2 x 0.2" hole	NaI crystal water cooled magnetic shielding	Test section, full and empty with interpolation. Lucite void models	One shot measurements	0.01
(10 and 11) 3/58	Vertical upflow of air - water mixtures	Lucite, rectangular cross-sections 2 x 1/8", 1/4", 1/2", 3/4", 1" - all 4' long	Ambient temperature Atmospheric pressure Water velocity, 1 to 10 fps. Mass flux, 2.5×10^5 to 20×10^5 lb/hr-ft^2	thulium-170 (0.085 mev peak) Pellet 0.19" diam 9 r/hr @ 6"	NaI thallium activated scintillation crystal, RCA 5819 photo-multiplier tube. Lucite light pipe between crystal and tube. Linear current amplifier, Brown 0-10 mv recorder. Beam collimated at tube by Pb window 1" thick with slot 1/32" x 2". NaI crystal cooled by water coils.	Lucite mockups of 2-phase flow patterns, annular flow, local boiling, parabolic distribution of voids in liquid, homogeneous flow.	One shot, local traverse longitudinal traverse	0.1
(12) 8/58	Vertical upflow of air - water mixtures	0.724" ID glass tube 5' long	Ambient pressure and temperature	thulium-170 0.01" diam x 1-1/8" long, 0.9 μc				
(13) 11/58	Vertical upflow of steam - water	stainless steel, rectangular 1/2" x 2". 1/8" thick wall, electrically heated	No Data	thulium-170 (0.085 mev peak) Pellet 0.19" diam 9 r/hr @ 6" collimated by 1/2" diam hole	Baird Atomic 8125 scintillation probe. Baird Atomic 131 scaler.	Test section full and empty interpolate in-between. Check against quick closing valves to trap flowing mixture.	One shot and local traverse	No Data
					NaI thallium activated crystal, 1-1/4" diam x 1" thick. RCA 5819 or Dumont 6292 photo-multiplier tube detector shielded by MU-metal against mag field and Pb shield against background and scatter, water-cooled detector, beam collimated at crystal by 1/2" x 5/8" Pb window.	Lucite mockups and interpolation based on full and empty reading of test section	One shot and longitudinal traverse	No Data
(14) 12/58	Horizontal flow of air - water mixtures	Lucite, rectangular cross-sections, 2 x 1/8", 1/4", 1/2", 3/4", and 1". Test section length 10'.	Ambient temperature, atmospheric pressure, quality 0.0005 to 0.0517 W_{H_2O}/W_{air}, 0.3 to 3.66 lb/sec W_{air}, 0.001 to 0.06 lb/sec.	thulium-170 (0.085 mev peak) Pellet 0.2" diam 9 r/hr @ 2"	Same as 10. Beam collimated at crystal by 1/2" x 5/8" window or 1/32" x 1/2" window. Large window for one shot, small window for traversing.	9 different Lucite mockups	One shot and local traverse across a given cross-section Longitudinal traverse along length of test section.	0.09 local traverse, 0.01, one shot 0.09

REFERENCES

γ-Ray Attenuation

1. K. Schwarz, "Investigation of Density Distribution, Water and Steam Velocities, as Well as Pressure Loss in Vertical and Horizontal Upflow Boiler Tubes," VDI Forshunpheft 445, Ed B, 20 (1954) pp 1-44

2. R. R. Rhode, and W. H. Cook, "Effect of Preferred Void Distributions on Void Measurements," ANL-5462 (April 1955)

3. R. V. Bailey, P. C. Zmola, F. M. Taylor, and R. J. Planchet, "Transport of Gases Through Liquid-Gas Mixtures," CF-55-12-118 (December 21, 1955)

4. W. H. Cook, "Boiling Density Studies in Multiple Rectangular Channels," BNL-2446 (December 1955)

5. J. F. Marchaterre, "The Effect of Pressure on Boiling Density in Multiple Rectangular Channels," ANL-5522 (February 1956)

6. W. H. Cook, "Boiling Density in Vertical Rectangular Multi-Channel Sections with Natural Circulation," ANL-5621 (November 1956)

7. H. S. Isbin, U. C. Sher, and K. C. Eddy, "Void Fractions in Two-Phase Steam Water Flow," J. A.I. Ch. E., 3 (1957) p 136-42

8. R. A. Egen, D. A. Dingee, and J. W. Chastain, "Vapor Formation and Behavior in Boiling Heat Transfer," BMI-1163 (March 4, 1957)

9. M. Richardson, and A. S. Kitzes, "Evaluation of Gamma-Ray Attenuation Techniques for Measuring the Density and Homogenity of Thorium Oxide Slurries Circulating at 300°C," CF-57-10-61 (1957)

10. M. Petrick, and B. S. Swanson, "Radiation Attenuation Method of Measuring Density of a Two-Phase Liquid," Rev. of Sci. Instr., 29, (1958) p 1079-85

11. M. Petrick, "Two-Phase Air-Water Phenomena," ANL-5787 (March 1958)

12. F. DeWinter, "Gamma-Ray Techniques for the Determination of Distribution Functions in Two-Phase Flow in a Vertical Tube," M.I. T., S.B. Thesis (August 1958)

13. H. H. Hooker, and G. F. Popper, "A Gamma-Ray Attenuation Method for Void-Fraction Determinations in Experimental Boiling Heat Transfer Test Facilities," ANL-5766 (November 1958)

14. B. L. Richardson, "Some Problems in Horizontal Two-Phase Two Component Flow," ANL-5949 (December 1958)

15. H. Buchberg, et al., "Studies in Boiling Heat Transfer — Final Report," COO-24 (March 1951)

16. M. L. Greenfield, et al., "Studies on Density Transients in Volume Heated Boiling Systems – Final Report," AECU-2950 (October 1954)

17. E. W. Grohse, "Analysis of Gas-Fluidized Solid Systems by X-Ray Absorption," J. A.I. Ch. E., 1 (1955) p 338

18. Ball, Lanmuir, and Wright, "X-Ray Measurement of Time Varying Steam Void-Fraction in a Thin Water Channel," RW-RL-137 (1959)

19. R. F. Kemp, A. L. Morse, R. W. Wright, and S. M. Zivi, "Kinetic Studies of Heterogeneous Water Reactors," RWD-RL-167 (February 29, 1960)

β-Particle Absorption

20. E. W. Groshe, Gen. Elec. Res. Lab. Rept., RL-1218 (December 1954)

21. D. Anson, R. E. Belin, and M. L. Harlor, Dept. Sci. Ind. Research, Dominion Physical Lab. Rept. R239, Lower Hath, New Zealand (February 1955)

22. E. English, P. T. Blacker, and W. E. Simmons, AERE Ed/M 20 (1955)

23. C. P. Costello, "Aspects of Local Boiling Effects on Density and Pressure Drop," ASME Paper No. 59-H-18 (August 1959)

Photographic

24. F. C. Gunther, "Photographic Study of Surface Boiling Heat Transfer to Water with Forced Convection," Trans ASME 73 (1951) p 115

25. P. Griffith, J. A. Clark, and W. M. Rohsenow, "Void Volumes in Subcooled Boiling Systems," ASME Paper 58-HT-19

Radioactive Tracer

26. C. E. Dengler, Ph.D. Thesis, M.I.T. (1952)

General References

27. G. W. Grodstein, "X-Ray Attenuation Coefficients from 10 kev to 100 Mev," NBS-583 (1958)

28. R. Rockwell, "Reactor Shielding Design Manual," TID-7004 (March 1956)

29. R. K. Swank, "Characteristics of Scintillators," Ann. Rev. Nuclear Science 4, (1954) p 114

REFERENCES

30. W. P. Ball, R. Booth, and M. H. MacGregor, "Scintillation Temperature Coefficients," Abstracts of the American Physical Society Meeting at Washington

31. F. W. Kinard, "Temperature Dependence of Photomultiplier Tube Gain," Nucleonics, 15 (1957) p 92

32. P. Griffith, and G. B. Wallis, "Slug Flow," M.I.T., DSR Rept. 7-7673 (May 1959)

33. R. Moissis, "Entrance Effects in a Developing Slug Flow," Sc. D. Thesis, M.I.T. (May 1960)

34. G. J. Hine, and G. L. Brownell, "Radiation Dosimetry" (1958)

35. S. W. Gouse, "Boiling Heat Transfer," AI-TDR-5652

36. S. W. Gouse, "Methods of Measuring Void Fractions," AI-TDR-5597

37. D. S. Duncan, "Void Fraction Detection in Santowax R," AI-TDR-5624

38. W. H. Wickes, "System Description of Flow Stability Test Loop," NAA-SR-TDR-6874

39. Atomics International, "Annual Technical Progress Report," NAA-SR-6730, (FY 1961)

40. W. P. Kunkel, "A Survey of the Assumptions and Areas of Uncertainty in OMR Hazards Evaluation," NAA-SR-TDR-6006